ACS APPLIED MATERIALS & INTERFACES

www.acsami.org

Research Article

Nanostructured Non-Newtonian Drug Delivery Barrier Prevents Postoperative Intrapericardial Adhesions

Xichi Wang, Zongtao Liu, Diego A. Sandoval-Salaiza, Samson Afewerki, Mildred G. Jimenez-Rodriguez, Lorena Sanchez-Melgar, Gabriela Güemes-Aguilar, David G. Gonzalez-Sanchez, Oscar Noble, Cecilia Lerma, Roberto Parra-Saldivar, Dario R. Lemos, Guillermo A. Llamas-Esperon, Jiawei Shi, Li Li, Anderson O. Lobo, Andres A. Fuentes-Baldemar, Joseph V. Bonventre,* Nianguo Dong,* and Guillermo U. Ruiz-Esparza*

Cite This: https://doi.org/10.1021/acsami.0c20084

Read Online

ACCESS | Metrics & More | Article Recommendations | Supporting Information

ABSTRACT: With the increasing volume of cardiovascular surgeries and the rising adoption rate of new methodologies that serve as a bridge to cardiac transplantation and that require multiple surgical interventions, the formation of postoperative intrapericardial adhesions has become a challenging problem that limits future surgical procedures, causes serious complications, and increases medical costs. To prevent this pathology, we developed a nanotechnology-based self-healing drug delivery hydrogel barrier composed of silicate nanodisks and polyethylene glycol with the ability to coat the epicardial surface of the heart without friction and locally deliver dexamethasone, an anti-inflammatory drug. After the fabrication of the hydrogel, mechanical characterization and responses to shear, strain, and recovery were analyzed, confirming its shear-thinning and self-healing properties. This behavior allowed its facile injection (5.75 ± 0.15 to 22.01 ± 0.95 N) and subsequent mechanical recovery. The encapsulation of dexamethasone within the hydrogel system was confirmed by ^{1}H NMR, and controlled release for 5 days was observed. *In vitro*, limited cellular adhesion to the hydrogel surface was achieved, and its anti-inflammatory properties were confirmed, as downregulation of ICAM-1 and VCAM-1 was observed in TNF-α activated endothelial cells. *In vivo*, 1 week after administration of the hydrogel to a rabbit model of intrapericardial injury, superior efficacy was observed when compared to a commercial adhesion barrier, as histological and immunohistochemical examination revealed reduced adhesion formation and minimal immune infiltration of CD3+ lymphocytes and CD68+ macrophages, as well as NF-$\kappa\beta$ downregulation. We presented a novel nanostructured drug delivery hydrogel system with unique mechanical and biological properties that act synergistically to prevent cellular infiltration while providing local immunomodulation to protect the intrapericardial space after a surgical intervention.

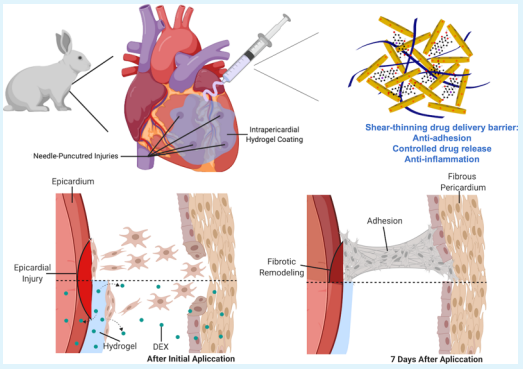

KEYWORDS: *nanotechnology, nanomedicine, self-healing hydrogel, controlled drug release, postoperative intrapericardial adhesions*

INTRODUCTION

Intrapericardial adhesions secondary to surgical interventions have become a serious medical problem with life-threatening consequences that affect 7−9% of patients who undergo multiple cardiac operations in the United States, and adhesiolysis represents an estimated annual total cost of 2.3 billion for the US healthcare system.[1−3] With the advent of new procedures and technologies that require multiple surgical interventions to treat cardiovascular pathologies or that serve as a bridge to transplantation such as the implantation of left ventricular assisting devices, the incidence of intrapericardial adhesion cases with moderate and serious consequences has increased.[4] Patients that present this pathology report poorer clinical outcomes, prolonged duration of hospitalization, and higher medical costs.[2,5]

A multifactorial cascade of ischemia, inflammation, angiogenesis, and tissue repair is responsible for the formation of postoperative intrapericardial adhesions.[1,6] During cardiac surgical interventions, pericardial injury is produced with subsequent loss of mesothelial lining, bleeding, and increased vascular permeability.[7] This results in the extravasation of the fibrinogen-rich fluid from the injured surfaces to the exposed sub-mesothelial connective tissue, where fibrin forms and

Received: November 13, 2020
Accepted: March 10, 2021

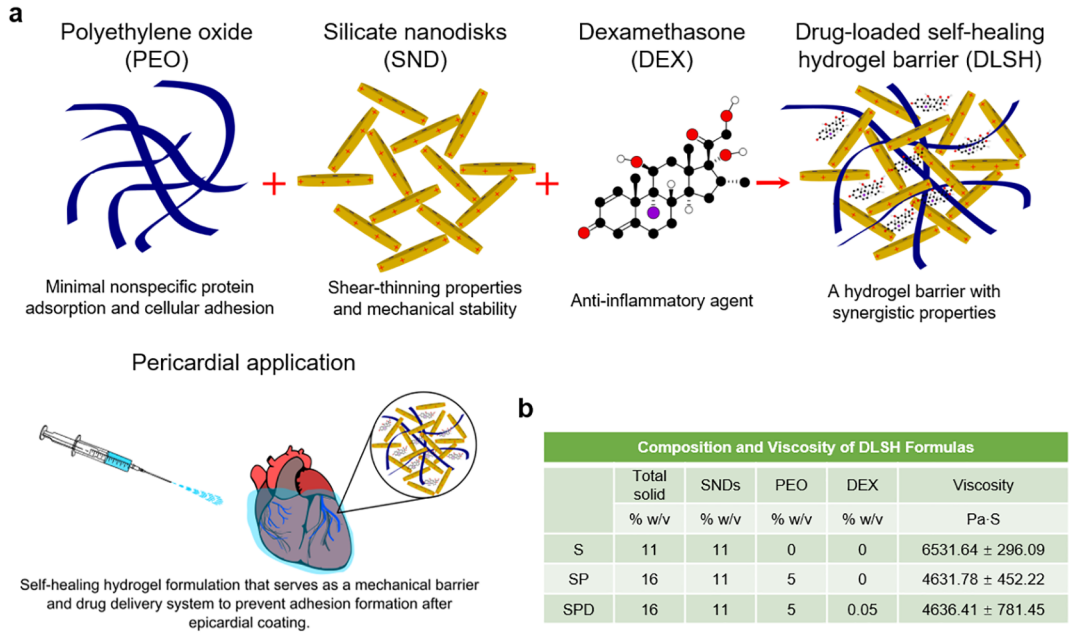

b

Composition and Viscosity of DLSH Formulas					
	Total solid	SNDs	PEO	DEX	Viscosity
	% w/v	% w/v	% w/v	% w/v	Pa·S
S	11	11	0	0	6531.64 ± 296.09
SP	16	11	5	0	4631.78 ± 452.22
SPD	16	11	5	0.05	4636.41 ± 781.45

Figure 1. Fabrication and rheological analysis of drug-loaded self-healing hydrogel (DLSH) formulations. (a) Schematic representation of DLSH synergistic components and the intrapericardial hydrogel application. (b) Hydrogel fabrication was performed by incorporating specific ratios of SNDs, PEO, and DEX, and their inherent viscosity was obtained after rheological characterization.

inflammatory cells adhere.[1,7,8] If fibrinolysis does not occur within 5 days, the fibrin matrix will persist and gradually become more organized as collagen-secreting fibroblasts migrate and lead the adhesion formation at the injury site.[6,9]

From a clinical standpoint, the formation of postoperative intrapericardial adhesions results in several negative implications, such as potential constrictive pericarditis and heart failure due to tissue friction, inflammation, and subsequent compromise of diastolic function.[10] Other common consequences include increased difficulty and duration of subsequent surgical procedures, as the surgeon needs to remove the fibrous tissue surrounding the mediastinal or epicardial spaces with the risk of inadvertently injuring the heart, great vessels, or other delicate anatomical structures.[11,12]

Several types of physical barriers in the form of films and membranes have been designed for abdominopelvic surgical procedures and translated to cardiovascular applications with several limitations; however, no technology has been exclusively designed for cardiovascular surgery, and several technical aspects limit the application and efficacy of traditional physical barriers in the pericardial space.[13,14] Some of the elements that limit the effective use of film-based physical barriers in cardiovascular surgery include incompatibility with minimally invasive interventions, challenging applications to irregular surfaces and cavities such as the mediastinal space, and potential fragility and disruption of the films as a result of the mechanical stress exerted by the beating heart.[15,16] Other approaches for the prevention of intrapericardial adhesions such as the application of surgical sealants or liquid-based solutions have been explored; nevertheless, several clinical studies have shown low efficacy.[17] Therefore, the development of novel technologies to solve these clinical limitations is urgently needed.

The ideal technology to prevent adhesion formation in the intrapericardial region should be designed to modulate the local inflammatory response, resist mechanical stress, uniformly cover the epicardial surface, and protect areas with the absence of mesothelial lining to impede infiltration of the collagen secreting cells responsible for the development of adhesions.

Based on these needs, self-assembling and self-healing hydrogel formulations could be especially attractive substitutes for commercially available barriers. In this study, we developed a nanostructured non-Newtonian hydrogel barrier specifically designed to prevent adhesions after cardiac surgery, and that serves as a self-healing physical cardiac membrane capable of withstanding the intrapericardial mechanical stress present during continuous cardiac pulsation without causing any friction. Additionally, the system has the capability to modulate the local inflammatory response by releasing an anti-inflammatory agent.

To design an efficient self-healing physical barrier, silicate nanodisks (SNDs) of 25 nm × 0.92 nm in size were selected for their unique mechanical properties that allow their self-assembly into a fractal network that resembles a "house of cards" superstructure and nanosized mesh to prevent the passage of molecules. The unique physical configuration of these nanostructures enables the formation of a non-Newtonian hydrogel barrier system that provides continuous and immediate mechanical recovery (self-healing) during pulsating stress due to the electrostatic attraction of the positively charged edges and negatively charged surfaces of SNDs.[18]

Polyethylene oxide (PEO) was introduced into the hydrogel formulation to inhibit nonspecific protein adsorption and cellular adhesion due to a surface steric exclusion mechanism, protecting tissues from cellular infiltration and protein deposition.[14] Furthermore, we incorporated dexamethasone (DEX) into the system, an insoluble anti-inflammatory drug usually administrated in the perioperative period of cardiovascular surgery to improve surgical outcomes.[19]

Based on this design, we envision a unique and versatile nanoplatform that can be applied via multiple delivery methods

https://doi.org/10.1021/acsami.0c20084
ACS Appl. Mater. Interfaces XXXX, XXX, XXX−XXX

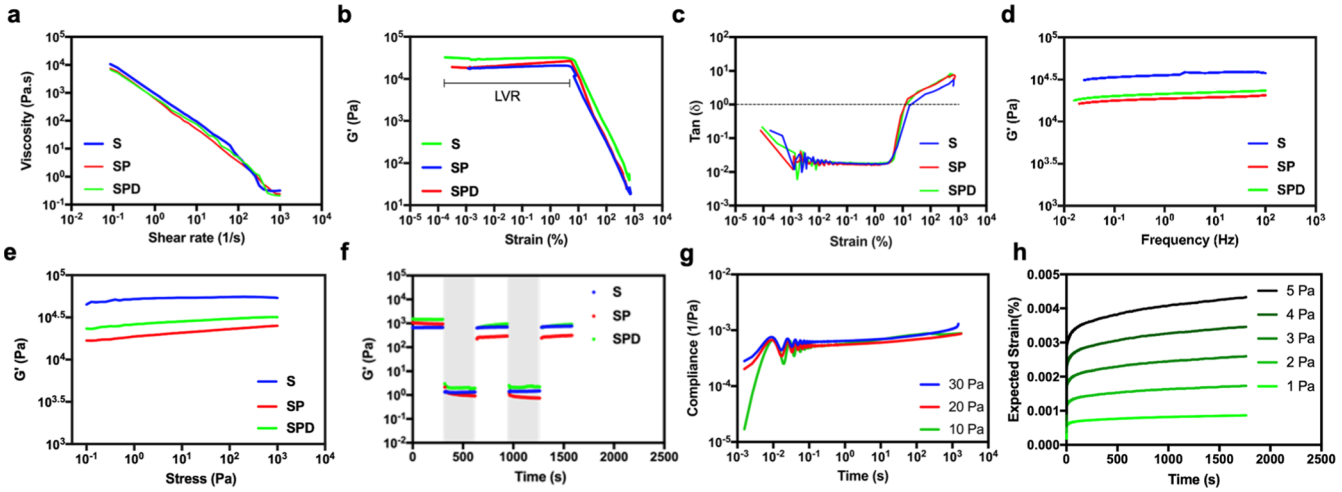

Figure 2. Rheological analysis of DLSH formulations. (a) Shear-thinning properties were confirmed as decreased viscosity was observed when hydrogel compositions were exposed to increased amounts of shear rate. (b) Storage moduli (G') *vs* strain (0.001−1000% at 1 Hz) was measured to define the linear viscoelastic regions (LVRs) of the hydrogel compositions. (c) The gel point [tan (δ) = 1] was found at ∼10% strain, after tan (δ) *vs* strain was quantified. (d) Storage moduli (G') *vs* frequency (0.01−100 Hz at 1% strain) measurements confirmed hydrogel stability. (e) Storage moduli (G') *vs* stress (0.1−1000 Pa) test did not result in any significant mechanical changes of DLSH formulations. (f) During the application of multiple strain cycles of low (1%) and high (100%) intensity to the hydrogel compositions, storage moduli (G') was recorded. As observed in the light gray regions of the plot, hydrogels presented a rapid recovery to their original modulus after each cycle. (g) The compliance *vs* time plot demonstrates the viscoelastic properties of SPD formulation after the application of 10, 20, and 30 Pa. (h) The plot depicts a stable creep response after exposing SPD formulation to expected physiological strain levels. Rheological characterization was measured in triplicate and representative data are shown.

in a more practical and efficacious manner. We hypothesized that this rationally designed nanostructured hydrogel technology, composed of ingredients that act synergistically to provide unique mechanical and biological features, will provide a novel approach that can ultimately prevent the formation of intrapericardial adhesions and overcome the current technical limitations of other technologies.

RESULTS AND DISCUSSION

Hydrogel Rapidly Recovers Its Mechanical Integrity after the Application of Stress, Strain, and Creep. The development of intrapericardial technologies to protect the heart after surgical interventions from fibrotic formations is an attractive and clinically relevant approach to decrease adhesion-associated morbidity and improve surgical outcomes. With the advent of nanotechnology and the availability of smart biomaterials that could serve as building blocks to fabricate a self-healing physical barrier able to withstand the shear generated by a beating heart, we envisioned the formulation of a nanostructured hydrogel technology able to coat the epicardial surface and continuously self-heal. The system was designed to disassemble and reassemble to its original physical state after every heartbeat, serving as a dual functional hydrogel system that simultaneously serves as a physical barrier and a drug delivery platform to prevent adhesion formation.

To achieve these unique mechanical properties, a nanostructured hydrogel was designed by incorporating biodegradable SNDs with an average size of 25 nm and a total electrostatic charge of −22.4 mV (Figure S1) in conjunction with PEO and DEX. This combination resulted in the creation of a drug-loaded self-healing hydrogel (DLSH) barrier (Figure 1a). The incorporation of SNDs into the hydrogel system provides a shear-thinning behavior that, in conjunction with the antifouling properties of PEO and the anti-inflammatory effect of DEX, results in the formation of a robust and simple platform for the formulation of a smart self-healing physical barrier with drug delivery capabilities.

The shear-thinning and self-healing properties of DLSH were confirmed by rheological analysis, as shear rate, strain sweep, stress sweep, frequency, creep, and recovery tests were performed. Three hydrogel formulations composed of SNDs (S), SNDs with PEO (SP), and SNDs with PEO and DEX (SPD) were fabricated and characterized to determine the physical and mechanical effect of each individual component (SNDs, PEO, and DEX) (Figure 1b).

Hydrogel formulations were exposed to different shear rates (0.1−1000 s^{-1}) to determine their viscosity and shear-thinning capabilities. Figure 2a confirms the non-Newtonian behavior of the hydrogel compositions as their viscosity decreased when shear rate was increased. It was observed that the incorporation of PEO into SP and SPD formulations caused a slight decrease in the initial viscosity of the hydrogel systems without affecting their shear-thinning properties. Furthermore, sweep strain analysis was performed at a strain of 0.0001−1000% (1 Hz) to determine the linear viscoelastic region (LVR) of the hydrogel materials. The LVR was found to be between 0.0001 and 10.0 strain (%) as shown in Figure 2b. Once the LVR was known, additional rheological experiments (stress sweep and frequency sweep) were conducted within this range. A decrease in storage modulus (G') was observed after the LVR of the hydrogel compositions; this decrease results from the disassembly of SNDs when the physical crosslinking is disrupted by high strain.[20] Additionally, to evaluate the gel point [tan (δ) = 1] of the hydrogel formulations, tan (δ) *versus* strain was recorded.[21] The gel point was detected at ∼10 strain percentage for the three hydrogel compositions. Higher elasticity was observed when the strain percentage was below 10 (tan (δ) <1), and when the strain percentage was higher than 10 [tan (δ) > 1], viscosity increased (Figure 2c).

https://doi.org/10.1021/acsami.0c20084
ACS Appl. Mater. Interfaces XXXX, XXX, XXX−XXX

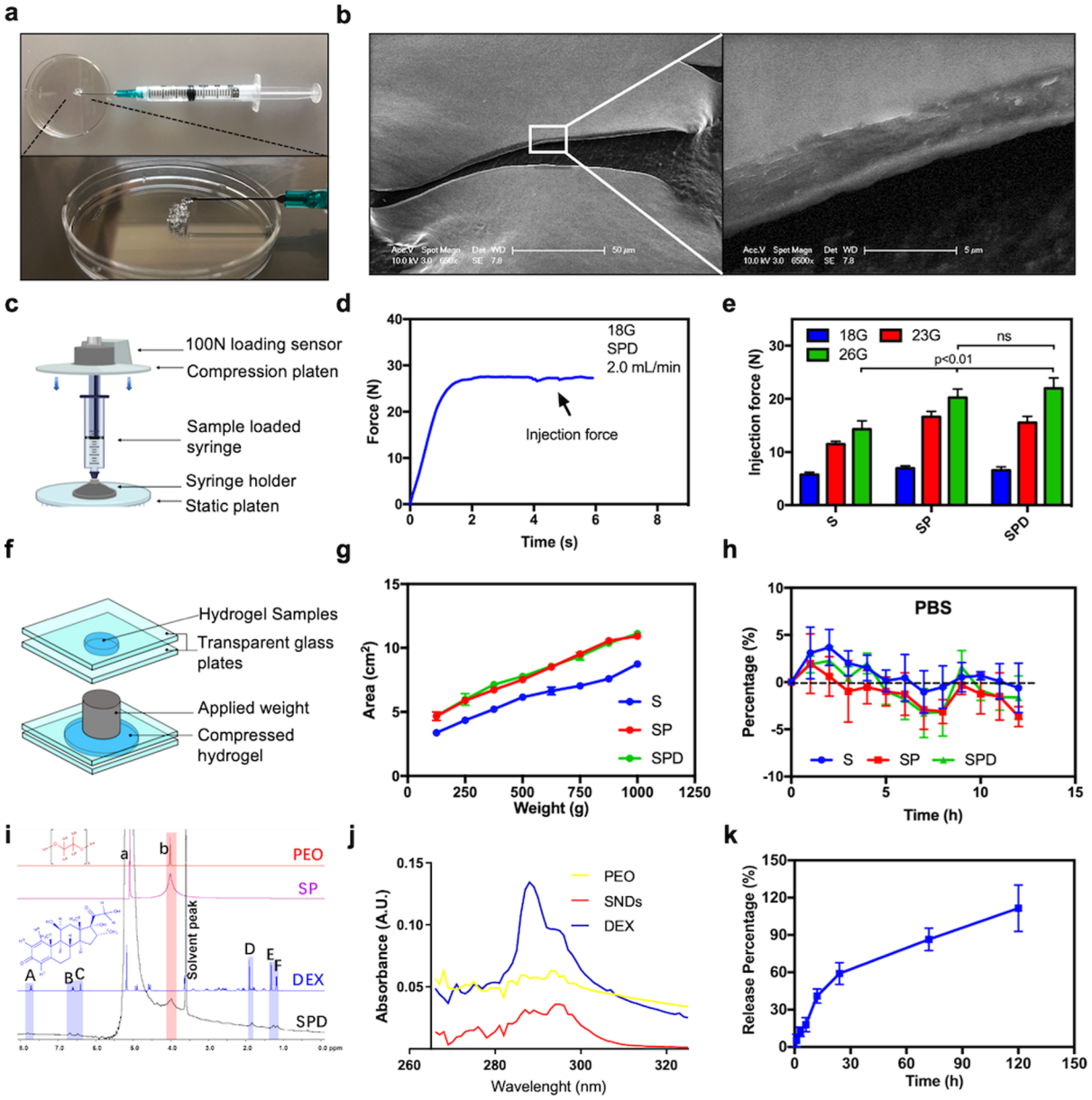

Figure 3. DLSH application, swelling, and release kinetics. (a) The SPD hydrogel formulation can be observed after extrusion. (b) Scanning electron micrograph of SPD formulation. (c) Schematic representation of the mechanical tester setup used to compress the syringe plunger and record the extrusion force. (d) Extrusion force (N) *vs* time was recorded, and the plateau (arrow) indicates the maximum required force to extrude the hydrogel formulation from the syringe. (e) Injection force of DLSH formulations was determined in 18G, 23G, and 26G needles; (f) schematic representation of the compression system used to evaluate the spread area of DLSH formulations. (g) After compressing the DLSH formulations for 5 min at 37 °C, SP and SPD hydrogels showed higher spreadability. (h) After phosphate-buffered saline (PBS) incubation at 37 °C, DLSH compositions did not swell more than 5% of their original weight. (i) ^{1}H NMR spectra of PEO, SNDs, and DEX were obtained. The ^{1}H NMR spectra confirmed the presence of each component of the SPD formula. (j) UV−vis absorbance of DEX (285 nm) in comparison to PEO and SNDs absorbance. (k) DEX release kinetics from the SPD formula extended for 5 days, as plotted after UV−vis spectroscopy quantification. Data analysis is presented as mean ± SD, $n = 5$ for (e). $n = 3$ for (g−k). *P*-values were obtained via Student's *t*-test (ns: $P > 0.05$) and one-way analysis of variance (ANOVA).

To prove the stability of the hydrogel formulations, the frequency of G' was recorded at predetermined ranges (0.01−100 Hz).[22] In Figure 2d, it can be observed that the different formulations remained intact during the frequency assessment. The hydrogel composition that solely contained SNDs (S) displayed the highest gel strength in comparison to other nanocomposite formulations incorporated with PEO and DEX (SP and SPD) that presented a decrease in G'. The decrease in G' of SP and SPD correlates with the weakening of the surface-edge physical interaction between the SNDs as a consequence of the addition of other components to the formulation (PEO and/or DEX) and their subsequent adsorption and intercalation between the SNDs.[23,24] A similar trend was observed when the frequency was altered to stress sweep, where formulation S ($G' \approx 53717.5$ Pa at 1 000 Pa) displayed the highest storage modulus, followed by SP ($G' \approx 25147.8$ Pa at 1 000 Pa) and SPD ($G' \approx 31860.2$ Pa at 1 000 Pa) (Figure 2e). However, all formulations maintained mechanical integrity as a result of the intramolecular forces of SNDs and the other components.[25]

https://doi.org/10.1021/acsami.0c20084
ACS Appl. Mater. Interfaces XXXX, XXX, XXX−XXX

The self-healing ability and recoverability of DLSH formulations (S, SP, and SPD) were investigated by monitoring G' over multiple cycles of low (1%) and high (100%) strain (inside and outside the LVR) at 1 Hz. Figure 2f shows that over multiple strain cycles, the DLSH formulations recovered their initial modulus and mechanical properties demonstrating their high stability and self-recovery capacity.

To predict the behavior of DLSH compositions under the high creep present in the intrapericardial space, rheological determination of creep compliance was performed. The data presented in Figures 2g and S2 confirmed that the viscoelastic behavior of all DLSH formulations did not change over time.[26]

In this context, to determine the stability of DLSH formulations, higher shear stress than the one found on physiological conditions was used to mimic and surpass biological systems such as the peripheral and cardiac vasculature. The *in vivo* shear stress faced along the peripheral vascular walls is generally in the range of 0.5−1.2 Pa depending on the anatomical location.[27,28] The behavior of DLSHs along the cardiac vasculature was calculated by considering the physiological vascular stress (1−7 Pa), and the expected creep responses at lower stress values (1−5 Pa) were determined following a published procedure.[29,30] Creep compliance was determined by applying a much higher creep range (up to 20 Pa) to DLSHs, and this was further employed to extrapolate the expected physiological strain at 1−5 Pa; the mechanical stability of SPD formulation was confirmed under these conditions (Figure 2h), and a similar stability behavior was observed for S and SP compositions (Figure S2).

These results are relevant from a cardiac perspective as DLSH is expected to be under continuous mechanical stress as a result of heart beating. The observed rheological and self-healing properties of DLSH formulations are mainly caused by the capability of SNDs to disassemble when shear stress is applied and instantly reassemble to its original conformation when shear stress is removed, a well-documented behavior of this nanomaterial type.[31]

DLSH Presents Homogeneous Morphological Features. Environmental scanning electron microscopy (eSEM) was used to study DLSH morphological features and determine its homogeneity after fabrication. The hydrogel was placed and sectioned at the top of a substrate for subsequent imaging. In Figure 3a,b, hydrogel extrusion from a syringe can be observed, as well as electronic micrographs and their magnifications, showing a homogeneous hydrogel surface with smooth texture, flat surface, and sharp margins. These results suggest that DLSH components are homogeneously distributed within the hydrogel system, as neither aggregates nor crystals were observed. A cohesive hydrogel structure without any phase separation confirmed the adequate interconnectivity and electrostatic crosslinking between the SNDs, PEO, and DEX.

Shear-Thinning Properties Enable DLSH Extrusion. The invention of injectable adhesion barriers compatible with minimally invasive interventions, such as thoracoscopy, could benefit a broad population of patients with cardiac and other thoracic related pathologies, as current film-based adhesion barriers are incompatible with these types of procedures.

To demonstrate the injectability of DLSH and its potential application in minimally invasive interventions, the injection force required to extrude the hydrogels from syringes equipped with needles that possessed different intraluminal diameters (18G, 23G, and 26G) was evaluated (Table S1). A specialized setup was used to determine the hydrogel extrusion force during mechanical compression (2 mL/min) with a mechanical tester instrument (Figures 3c and S3). The maximum required force to extrude the hydrogels was detected after the force linearly increased and reached a plateau (Figure 3d).

As shown in Figure 3e, the extrusion force correlated with the needle size used was analyzed; needles with smaller intraluminal diameters required higher force compared to bigger sizes.

The force required to extrude the three different formulations when 18G, 23G, and 26G needles (intraluminal diameter: 0.84, 0.34 and 0.26 mm) were used was 5.75 ± 0.15 N, 11.51 ± 0.21 N, and 14.32 ± 0.55 N for S; 6.96 ± 0.14 N, 16.64 ± 0.36 N, and 20.24 ± 0.57 N for SP, and 6.57 ± 0.20 N, 15.53 ± 0.42 N, and 22.01 ± 0.95 N for SPD. Another factor that increased the extrusion force was the incorporation of PEO, as the formula that exclusively contained SNDs (S) required less force to be extruded. Unlike PEO, the incorporation of DEX into the formula (SPD) did not have a significant effect in the required extrusion force.

These results confirm the development of an injectable shear-thinning hydrogel that, from a mechanical perspective, addresses current clinical limitations, as it can be administered on injectable form, bypassing the physical and spatial restrictions that film-based barriers present during minimally invasive interventions.

DLSH Spreads as a Stable Barrier without Swelling. Spreadability is an important parameter to determine the intrapericardial coating capacity of DLSH. To assess the spreading performance of these hydrogel systems, we used a previously described method.[32] One milliliter of three different hydrogel formulas (S, SP, and SPD) was placed in the middle of two glass plates and compressed using different masses (125−1000 g) at 37 °C and at room temperature (Figure 3f). After 10 min of continuous compression, the diameter of each hydrogel formulation was measured, and the spreading area was calculated using the following equation:

$$\mathrm{Si} = d^2 \times \frac{\pi}{4} \tag{1}$$

Si accounts for the spreading area (cm^2) achieved by each hydrogel formulation after the application of different mass ranges (g) and d represents the mean diameter (cm) reached by the samples after compression. As shown in Figures 3g and S4, SP and SPD groups show a superior spread area compared to the S group. These data can be correlated with the results obtained from the rheological characterization of these formulations, as we can conclude that lower hydrogel viscosities result in higher spreading areas. In this case, SP and SPD formulas had lower viscosity and presented higher spreading area when compared to S. It is important to highlight that hydrogel formulations did not fracture under compression (Figure S4a).

To understand the mechanical stability of DLSH, a standardized procedure was used to determine the stiffness of each composition with the obtained spread area.[33] S, SP, and SPD were classified as very stiff gels, as their spread diameter was under 40 mm when a mass of 125 g was applied (Table S2).

To study the swelling behavior of hydrogel formulations in aqueous environments similar to the one present in the intrapericardial space, S, SP, and SPD were incubated at 37 °C on phosphate-buffered saline (PBS) and Dulbecco's modified

https://doi.org/10.1021/acsami.0c20084
ACS Appl. Mater. Interfaces XXXX, XXX, XXX−XXX

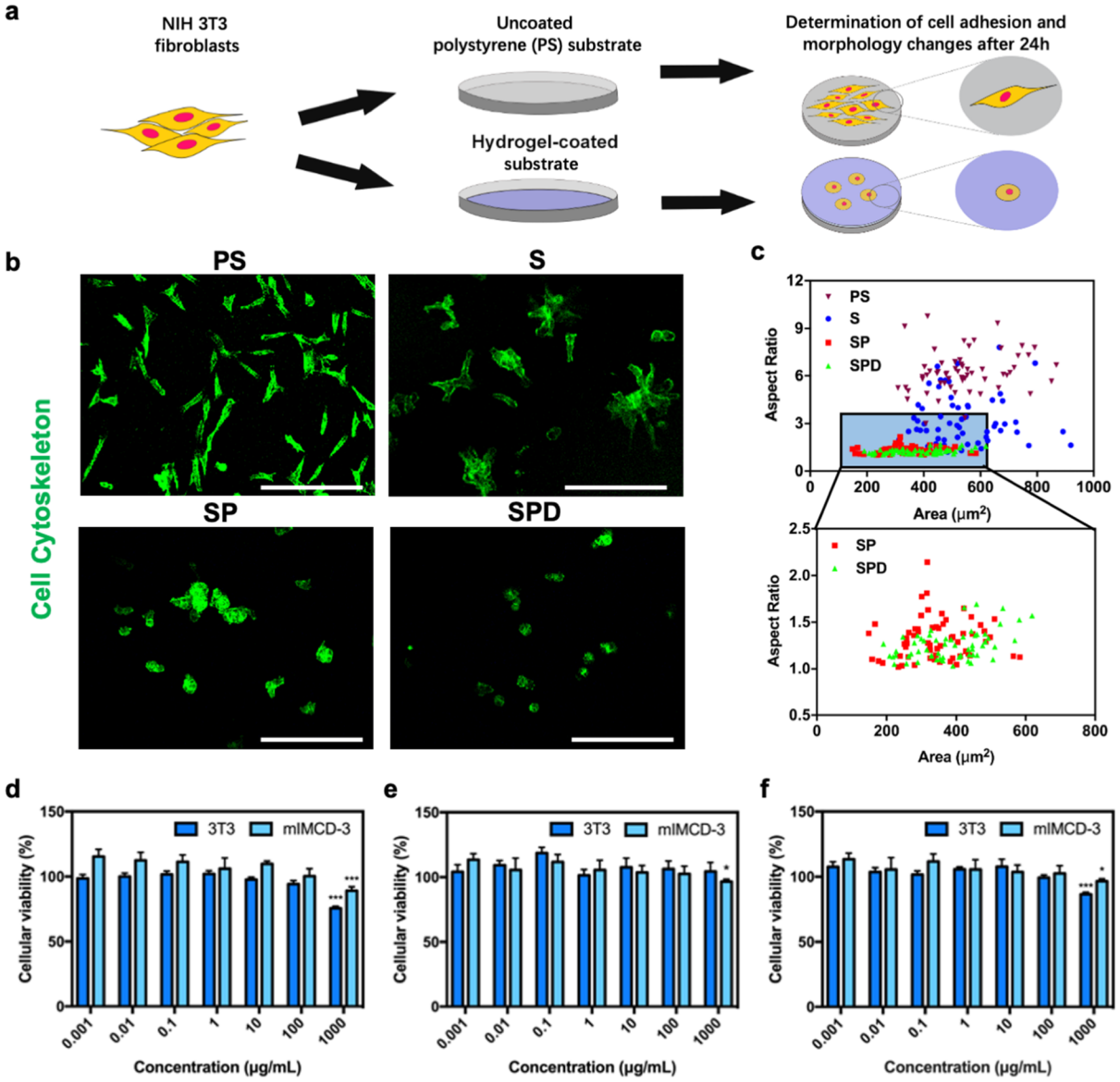

Figure 4. Characterization of cellular adhesion and biocompatibility of DLSH compositions. (a) Schematic representation of the experimental setup used to test cellular adhesion and morphological evaluation of 3T3 fibroblasts seeded under uncoated PS substrates and hydrogel-coated substrates (S, SP, and SPD) for 24 h. (b) Cellular morphology was evaluated in each substrate (PS, S, SP, and SPD) via confocal microscopy. Confocal micrographs showed limited cell membrane and pseudopodia expansion in SP and SPD groups compared to PS and S groups, where cellular expansion was normal. Scale bar = 50 μm. (c) Cell area and aspect ratio were quantified as measurements of cellular adhesion by membrane extension; it was determined that SP and SPD substrates presented a significantly reduced cell area and aspect ratio (light blue area) as a result of low cell adhesion when compared to PS and S groups. Cytotoxic determination of DLSH formulas was performed on NIH 3T3 fibroblasts and mIMCD-3 epithelial cells after 48 h of incubation on increasing hydrogel concentrations (0.001−1000 μg/mL); a slight decrease in cell viability was observed when S (d), SP (e), and SPD (f) concentrations were in the range of 1000 μg/mL. The data in this figure are expressed as mean ± SD, $n > 60$ for (c) and $n = 5$ for (d−f); P values were determined by using Student's t-test.

Eagle's medium (DMEM). Swelling behavior was determined at multiple timepoints over a 12 h period. Figure 3h shows that all hydrogel groups incubated in PBS presented a stable state with swelling below 5%. A similar behavior was observed when hydrogels were incubated on DMEM (Figure S5a). This evidence demonstrates that DLSH formulations can spread without significant swelling and form a robust physical barrier for intrapericardial administration and epicardial coating.

Degradation kinetics of the hydrogel formulations were analyzed after incubating the samples in PBS at 37 °C. After 14 days, the total percentage of mass loss of S, SP, and SPD formulations was 3.78% ± 0.98, 9.12% ± 1.09, and 6.92% ± 1.09, respectively (Figure S5b).

Other biomaterials could be used to create cohesive hydrogel systems such as carboxymethyl cellulose and hyaluronic acid; nevertheless, the superior self-recovery properties of SNDs allow better modulation of the viscoelastic properties of the hydrogel material and provide a more robust molecular barrier due to the intrinsic nanonetworks that these nanodisks create, preventing the passage of molecules like fibrin that could stimulate the formation of intrapericardial adhesions.[34,35]

https://doi.org/10.1021/acsami.0c20084
ACS Appl. Mater. Interfaces XXXX, XXX, XXX−XXX

DLSH Can Effectively Capture and Release DEX. DEX is a synthetic glucocorticoid used as an anti-inflammatory and immunosuppressant drug that is commonly applied in cardiovascular surgery.[19] To control the acute inflammatory response in the pericardial region after surgical intervention and to prevent adhesion formation, DEX was incorporated in the hydrogel formulation to immunomodulate the local microenvironment of the intrapericardial space.

SNDs were selected as drug delivery vehicles as their surface is suitable for molecular adsorption through hydrogen bonding; additionally, their intercalated conformation with interlayered spaces created after self-assembly can accommodate polar molecules and drugs such as DEX, tetracycline, doxorubicin, and itraconazole.[23,36−39] In Figure S6, it can be observed that despite its hydrophobic nature, DEX was solubilized in a SND solution after 12 h of stirring.

Proton nuclear magnetic resonance (^{1}H NMR) was utilized to verify the presence and incorporation of the different hydrogel components used during its fabrication. The loading capacity of DEX was confirmed to be 100%, as each component (SND, PEO, DEX) was individually analyzed and its respective spectra were employed to compare its presence through alignment with the spectra generated by the final hydrogel formulation (SPD). As depicted in Figure 3i and Table S3, the SPD hydrogel spectra show the presence of a peak corresponding to PEO (the protons ^{b}H in the PEO structure at δ = 3.84−3.43 ppm, m) and the presence of three protons (^{A}H, ^{B}H, and ^{C}H at δ = 7.64−7.44 ppm, br s, 6.49−6.33 ppm, br s, and 6.27−6.14 ppm, br s) and three methyl protons ($^{D}CH_3$, $^{E}CH_3$, and $^{F}CH_3$ at δ = 1.72 ppm, s, 1.15 ppm, s, and 1.05 ppm, s) corresponding to the DEX chemical structure.[40] Several studies have shown that anionic drugs, such as DEX, are attracted into the positively charged SND surface through hydrophobic interactions, hydrogen bonding, cation exchange, proton transfer, cation bridging, and anion exchange mechanisms.[41,42]

DEX release kinetics from SPD was studied by placing the hydrogel system inside a dialysis filter and incubating it on PBS (pH 7.4) at 37 °C under continuous shaking (Figure S7). At predetermined timepoints, UV−vis spectroscopy was used to determine the drug concentration of the dialysate, and the DEX maximal absorbance peak was located at 285 nm (Figure 3j). PEO and SNDs did not cause any interference during the spectroscopic detection. As shown in Figure 3k, the SPD formulation presented a sustained release profile of DEX for 120 h (5 days). This period is of particular importance since it corresponds to the initial phase of the acute inflammatory response that is responsible for the adhesion formation after a surgical intervention, longer release kinetics of DEX could affect wound healing, something our system will avoid.[43,44]

DLSH Prevents Cell Adhesion and Inflammation while Maintaining Its Biocompatibility. Cell−surface interactions exert a strong influence over cell function, and in the case of the pathophysiology of postoperative adhesions, they play a fundamental role in the adhesion, infiltration, and growth of fibroblasts.[45]

The characterization of cellular and material interactions is essential for the development of antiadhesion technologies that could limit adhesion formation. For this purpose, cellular adhesion, morphology, and growth of NIH 3T3 fibroblasts were evaluated on polystyrene (PS), S, SP, and SPD substrates via confocal microscopy after 24 h of incubation (Figure 4a). Cells seeded on PS (control) and S substrates presented a fusiform shape, an indicator of surface adhesion and pseudopodia expansion, as shown in the confocal micrographs (Figure 4b). In contrast, when the hydrogel compositions included PEO (SP and SPD groups), fibroblast morphology was observed to be rounded without any pseudopodia or other cellular membrane extensions, indicating poor attachment to the hydrogel surface.

Further evaluation was performed via single-cell analysis, fibroblast cytoskeleton was labeled, and confocal micrographs were obtained for additional morphological quantification (aspect ratio and cell area). The aspect ratio quantifies the size and dimension of an individual cell based on its geometrical shape and area, which are indicative of cell adhesion and expansion. When cells fail to attach to the substrate, their morphology will be spherical and the aspect ratio will be closer to 1, compared to adherent cells that present membrane expansion and irregular morphology and that result in an aspect ratio higher than 1.

In Figure 4c, single-cell analysis of different groups was performed. PS and S groups presented a significant difference ($p < 0.001$) in aspect ratio and cell area when compared to groups that contained PEO (SP and SPD). In contrast, SP and SPD groups showed a similar distribution with low aspect ratio and cell area due to the spherical shape of the cells, as a consequence of limited cellular adhesion and pseudopodia expansion. These results support the antiadhesion capabilities of PEO within the formulation and confirm the importance of antifouling materials for the design of self-healing physical barriers.

To establish that the limited cellular adhesion to the hydrogel compositions was not the result of a cytotoxic response to the material, a biocompatibility study was performed in 3T3 fibroblasts. Cells were incubated with increasing concentrations (0.001−1000 μg/mL) of S, SP, and SPD, and cellular viability was measured by spectrophotometric analysis as previously reported.[46] Minimal toxicity was observed in response to any of the hydrogel compositions after exposing the cells to high concentrations of these materials, confirming excellent biocompatibility (Figure 4d−f).

As a non-steroidal anti-inflammatory drug, DEX can attenuate acute inflammatory response and reduce immune infiltration by downregulating intercellular adhesion molecule 1 (ICAM-1) and vascular cell adhesion protein 1 (VCAM-1) on endothelial cells after a surgical intervention.[47] To mimic the acute inflammatory response *in vitro*, endothelial cells (bEnd.3) were seeded in different groups containing PBS, DEX (50 mM), SP, and SPD (50 mM) and stimulated with tumor necrosis factor alpha (TNF-α) (10 ng/mL). After 8 h of incubation, the cells were fixed, and the upregulation of key inflammatory adhesion molecules (ICAM-1 and VCAM-1) that mediate leukocyte recruitment was analyzed by immunohistochemistry and fluorescence microscopy.[48]

Figure 5a shows fluorescence micrographs of control (PBS), DEX, SP, and SPD groups without TNF-α treatment; ICAM-1 expression could not be observed. In contrast, some TNF-α-treated groups showed upregulation of ICAM-1 expression in Figure 5b. The control and SP TNF-α-treated groups presented higher upregulation of ICAM-1 compared to the DEX and SPD groups; this behavior is expected as DEX- and SPD-treated groups contain the anti-inflammatory compound, limiting the cellular inflammatory response.

In Figure 5c, the absence of VCAM-1 expression in non-stimulated endothelial cells can be observed; nevertheless, after

https://doi.org/10.1021/acsami.0c20084
ACS Appl. Mater. Interfaces XXXX, XXX, XXX−XXX

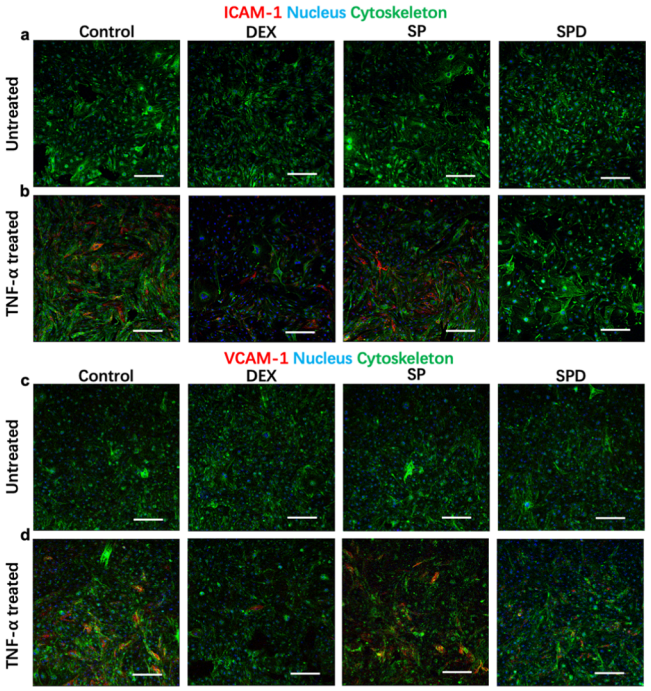

Figure 5. Cellular expression of inflammatory markers (ICAM-1 and VCAM-1) during DLSH treatment. Immunohistological examination of bEnd.3 endothelial cells stimulated with TNF-α was performed to evaluate the anti-inflammatory effect of the hydrogel formulations. (a) ICAM-1 expression was examined in control groups without TNF-α stimulation, resulting in no expression. (b) Control and SP groups treated with TNF-α showed increased upregulation of ICAM-1; in contrast, no significant upregulation was detected on DEX and SPD groups. (c) VCAM-1 expression was also determined in control groups without TNF-α stimulation resulting in no expression. (d) Similar to ICAM-1, VCAM-1 expression was attenuated when cells were treated with DEX and SPD. In contrast, VCAM-1 upregulation was detected on control and SP groups. Scale bar = 250 μm.

TNF-α stimulation, VCAM-1 expression was upregulated in control and SP groups as shown in Figure 5d. DEX and SPD groups showed attenuated VCAM-1 upregulation after TNF-α stimulation due to the anti-inflammatory effect from the drug compound. These results demonstrate that the incorporation of an anti-inflammatory drug such as DEX in the proposed hydrogel technology can modulate and reduce the inflammatory response of endothelial cells.[49]

Pericardial Adhesions Are Prevented after DLSH Administration. Pericardial postoperative adhesions can appear after cardiovascular surgical interventions.[7] In this study, we used an epicardial injury rabbit model to mimic the pathophysiology of adhesion formation and test the efficacy of DLSH as an intrapericardial physical barrier and drug delivery system (Figure 6a). For this purpose, three experimental groups were studied, a control group administered with saline solution (n = 5), a group administered with Seprafilm (n = 5), a commercially available physical barrier, and a group administered with the DEX-loaded SPD (n = 5).

After accessing the mediastinal cavity and the intrapericardial region, four epicardial injuries on the anterior ventricular wall were performed as previously reported.[50] Saline solution (control), Seprafilm, and SPD were applied inside the intrapericardial space of each group. After 7 days, animals were euthanized, and the thoracic incisions were reopened to determine the formation of postoperative adhesions (Figures 6b and S8). The excised hearts of the different groups can be clearly observed; control group administered with saline solution presented multiple adhesion formations in the surrounding areas of the injury sites; in contrast, a slight decrease in the formation of postoperative adhesions was observed when Seprafilm was used. Nevertheless, SPD formulation showed superior performance and efficacy as no postoperative adhesions were observed in the injured sites or the surrounding areas. When the excised hearts of the SPD group were analyzed, no pericardial adhesions were formed in the injury sites; instead, granulation tissue was found in accordance to the repair stage of wound healing.[51]

Figure 6c shows the average percentage of injury sites that developed fibrotic adhesions. Control and Seprafilm groups presented 95% ± 5 and 15% ± 6, in comparison to the SPD group that did not develop adhesions. The adhesion area was measured for each group resulting in an average of 1.05 ± 0.12 cm^2 for control, 0.2 ± 0.11 cm^2 for Seprafilm, and 0.00 ± 0.00 cm^2 for the SPD group (Figure 6d).

A modified version of the peritoneal adhesion index (PAI) was adapted and used to clinically evaluate the grade and severity of pericardial adhesions based on morphological features such as vascularization, thickness, and strength (Table S4).[52] In Figure 6e, it can be observed that the average adhesion score for the control group was around 9.4 ± 0.6, compared to Seprafilm that presented 1.4 ± 0.7 and 0.0 ± 0.0 for the SPD group as no adhesions were detected.

Physiological Tissue Remodeling and Decreased Immune Infiltration Observed after DLSH Administration. To determine tissue remodeling and investigate adhesion formation 7 days after conducting the surgical procedure, histopathological examination was performed on the excised pericardial region where the injuries were created.

Hematoxylin and eosin (H&E) staining was used to study morphological changes of the epicardium. As shown in Figure 7a, control and Seprafilm groups presented disruption of the epicardial lining and the formation of dense disordered fibrotic bands located in the intrapericardial region, more specifically in the areas where the surgical injuries were created. In contrast, the SPD group did not present fibrotic adhesion formations, as epicardial lining can be observed.

Masson's trichrome staining revealed the intrapericardial presence of dense fibrous bands containing scarce cells, adipose tissue, blood vessels, and collagen on the control and Seprafilm groups, confirming the formation of postoperative adhesions (Figure 7b). No intrapericardial collagen depositions or formation of fibrotic bands related to postoperative adhesions could be observed on the SPD group.

These histopathological observations correlate with the macroscopic evaluations of the peritoneal adhesion index (PAI) scoring system where adhesions in control and Seprafilm groups were classified as grade 3, and the SPD group did not present adhesion formations (grade 0). Based on these results, it can be confirmed that the SPD hydrogel offered a robust physical barrier by limiting cellular migration and collagen deposition in the intrapericardial space.

Immunohistological examination was used to analyze immune infiltration within the different experimental groups. DEX exerts most of its anti-inflammatory effect by inhibiting the NF-$\kappa\beta$ pathway responsible of proinflammatory cytokines activation and immune infiltration.[53] Figure 7c,d shows the infiltration of CD3-positive lymphocytes, CD68-positive macrophages, and the upregulation of NF-$\kappa\beta$ in the control

https://doi.org/10.1021/acsami.0c20084
ACS Appl. Mater. Interfaces XXXX, XXX, XXX−XXX

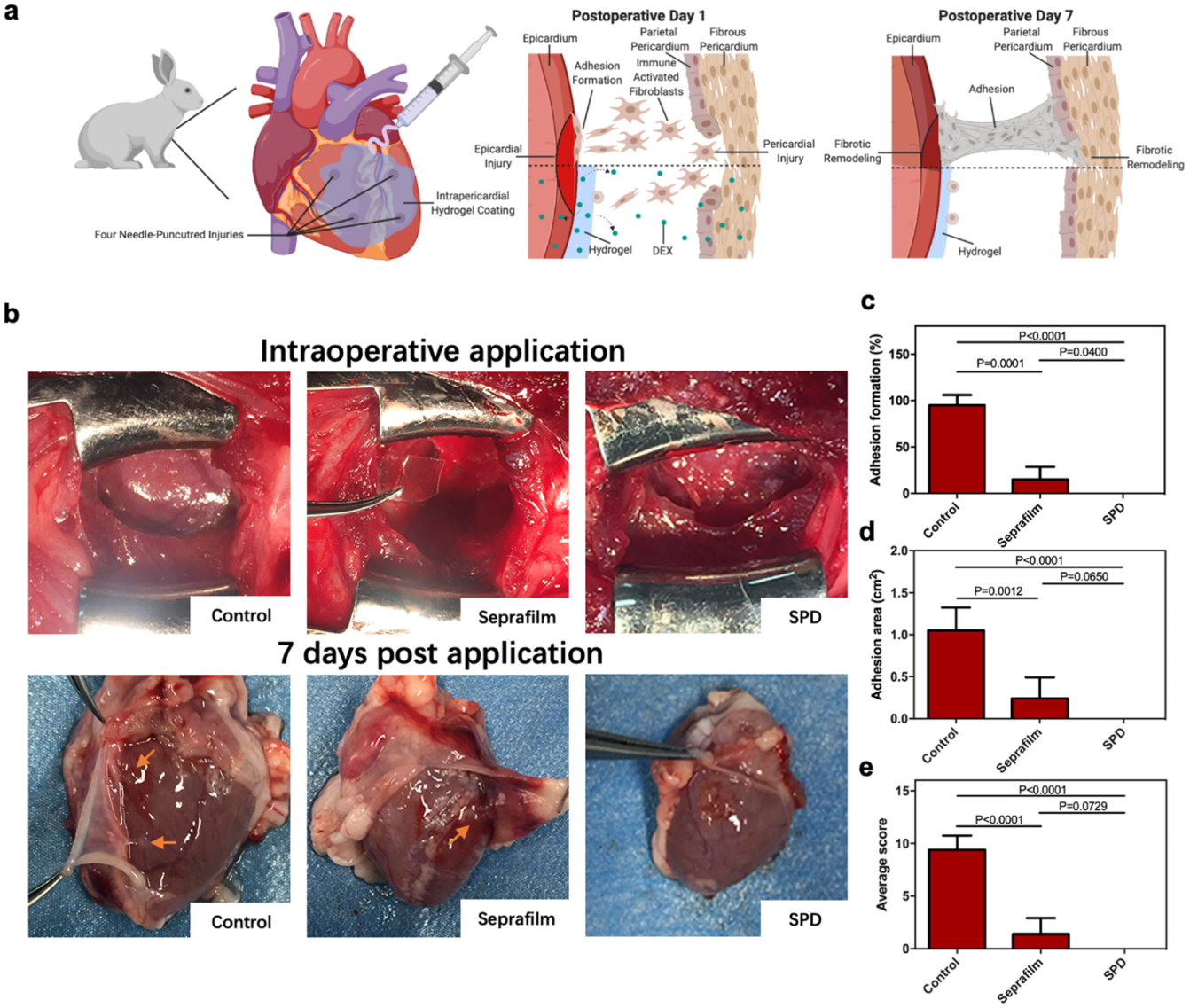

Figure 6. Comparative study to determine the DLSH efficacy to prevent postoperative intrapericardial adhesions. (a) The schematic depicts the administration of DLSH formulation to the injured intrapericardial space with the subsequent formation of a protective hydrogel coating in the epicardium that prevents adhesion formation compared to a non-treated heart. (b) Representative photographs of the epicardial administration of saline solution (control), Seprafilm, and SPD formulations to the injured sites. After 7 postoperative days, animals were euthanized and hearts were extracted to determine adhesion formations; the presence of fibrous adhesions (orange arrows) connecting the epicardium with the pericardium in control and Seprafilm groups was observed; in contrast, no adhesion formations were detected on the SPD group. (c) To determine the DLSH efficacy to prevent adhesions, the average percentage of adhesion formations was calculated; attenuation and prevention of adhesion formation were observed on Seprafilm and SPD groups, respectively. (d) The average adhesion area was measured; Seprafilm presented decreased adhesion formations by area, and SPD did not present any quantifiable adhesions. (e) A modified version of the PAI scoring system applied to the pericardium was used. The SPD group scored lower as no adhesion formations were found. The data in this figure are expressed as mean ± SD, n = 5 for (c−e). P-values were determined by using Student's t-test (ns: $P > 0.05$).

and Seprafilm groups. These observations confirm the presence of an inflammatory process that led to nascent fibrinous adhesions. Compared to the control and Seprafilm groups, the SPD-treated animals presented minimal immune infiltration and attenuation of NF-$\kappa\beta$ expression, as well as no progression to fibrotic formations. Quantification of C-reactive protein (CRP) and erythrocyte sedimentation rate (ESR) across the different groups was performed, and no significant differences indicative of a systemic inflammatory response were found (Figure S9a,b). These results demonstrate local immunomodulation of the postoperative acute inflammatory response when SPD is administered.

DLSH Does Not Interfere with Cardiac Function. Echocardiography was used to analyze cardiac function, as well as the presence of adhesions and the location of SPD in the intrapericardial space. Control, Seprafilm, and SPD groups were monitored preoperatively (day 0) and postoperatively (within the first hour and 7 days after the surgical procedure).

Figure 8a shows a preoperative echocardiographic image of an intact heart, where the pericardium and epicardium are well delimited and divided by the intrapericardial space without any pathological anomaly. After 7 postoperative days, the non-treated control group was echocardiographically reassessed; a pathological thickening of the pericardium and an echolucent

https://doi.org/10.1021/acsami.0c20084
ACS Appl. Mater. Interfaces XXXX, XXX, XXX−XXX

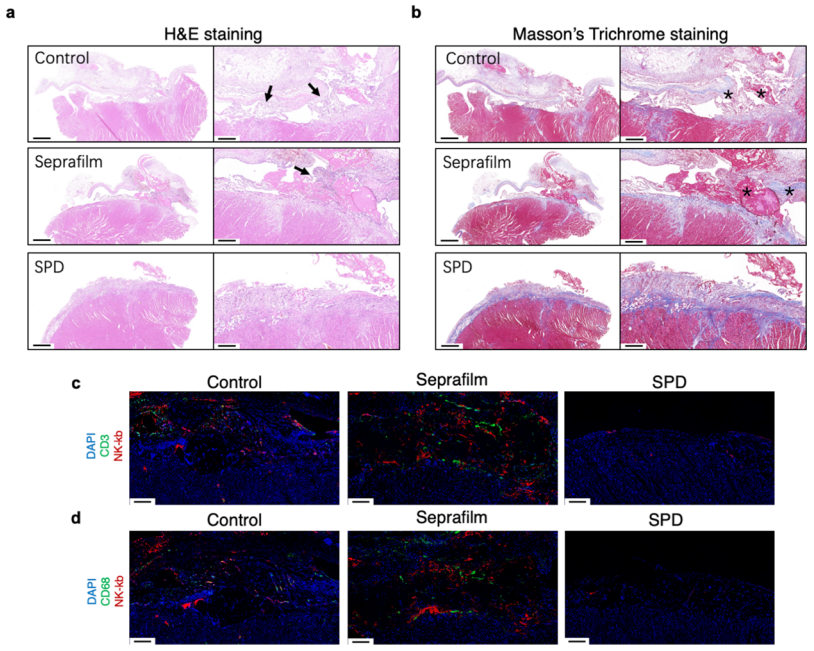

Figure 7. Histological analysis of tissue remodeling and intrapericardial inflammatory response. (a) H&E stained micrographs from epicardial tissue are presented (right column represents magnified tissue areas). In control and Seprafilm micrographs, the disruption of the epicardial lining and the formation of disordered fibrotic bands (arrows) connected to the pericardial region can be observed; in contrast, no postoperative adhesions were observed and preserved epicardial lining was found in the SPD-treated group. (b) Dense fibrotic bands composed of adipose tissue, blood vessels, collagen, and cells were detected (asterisks) in control and Seprafilm groups after Masson's trichrome staining was performed; SPD micrographs did not show intrapericardial adhesion formations or other types of collagen depositions. Immunohistological analysis of the different groups was used to understand lymphocyte (CD3) (c) and macrophage (CD68) (d) infiltration, as well as NF-κB upregulation. It can be observed that immune infiltration and NF-κB activation were observed in control and Seprafilm groups, compared to the DEX-loaded SPD hydrogel where immune infiltration and NF-κB activation were attenuated. Scale bars in (a,b) are 1 mm for left column micrographs and 400 μm for magnified insets (right column). Scale bars in (c,d) are 200 μm.

structure in the intrapericardial space were found and indicate the presence of fibrotic adhesions (Figure 8b and Movie S1). As a result of the inflicted pericardial and epicardial injury, an animal from the non-treated control group presented an echo-free signal that correlates with a pericardial effusion around the left ventricle and left atrium (Figure 8c). The presence of SPD in the intrapericardial space was confirmed after 1 h (Figure 8d) and 7 days (Figure 8e) of the surgical procedure. SPD was present in both timepoints and can be observed as a hyperechoic signal in the surface of the left ventricular epicardium within the intrapericardial space. A slight SPD deformation was observed during the echocardiographic study; nevertheless, the hydrogel system was able to recover its mechanical integrity and remain protecting the epicardial surface (Movie S2). After 7 days, no signs of postoperative adhesions were detected through echocardiography for the SPD group (Figure S10).

The cardiac function of the different groups (control, Seprafilm, and SPD) was assessed by echocardiographic analysis. Compared to the preoperative echocardiographic assessment (day 0), no significant differences in cardiac function were observed across the different groups at day 7 (Figure 8f–i). Mean left ventricular ejection fraction (LVEF), left ventricular internal diastolic diameter (LVIDd), left ventricular internal systolic diameter (LVIDs), and fractional shortening (FS) parameters were not impaired across the groups. In conclusion, ventricular systolic and diastolic function was preserved, and SPD did not restrict cardiac performance.

CONCLUSIONS

A novel nanotechnology-based hydrogel system has been introduced and characterized, it provides superior efficacy to prevent the pathophysiological formation of postoperative adhesions. This nanotechnology-based solution was developed to synergistically function as a physical barrier and a drug delivery system to prevent the onset of this disease.

Previously, several technologies composed of different cellulose derivatives or polytetrafluoroethylene have been developed with the aim of preventing the formation of postoperative adhesions; however, the patch-based configuration of these implants limits their application to minimally invasive interventions, and their poor mechanical properties and incompatibility with the challenging cardiac environment and anatomy result in low efficacy after cardiac surgery.[54,55]

The proposed hydrogel system in this article solves these clinical limitations, as its unique shear-thinning and self-healing mechanical properties allow its application in a wide variety of challenging anatomies and surgical modalities such as sternotomy, thoracotomy, and thoracoscopic procedures. This mechanical versatility, in conjunction with its anti-adhesion and anti-inflammatory effects, make this novel platform ideal for sternotomy as well as for minimal invasive procedures where the hydrogel can be applied through a small incision in the intrapericardial space without the total exposure of the heart or other mediastinal structures.

EXPERIMENTAL SECTION

Fabrication of a Self-Healing Drug Delivery Hydrogel. Hydrogels were formulated by creating several blends of SNDs

https://doi.org/10.1021/acsami.0c20084
ACS Appl. Mater. Interfaces XXXX, XXX, XXX−XXX

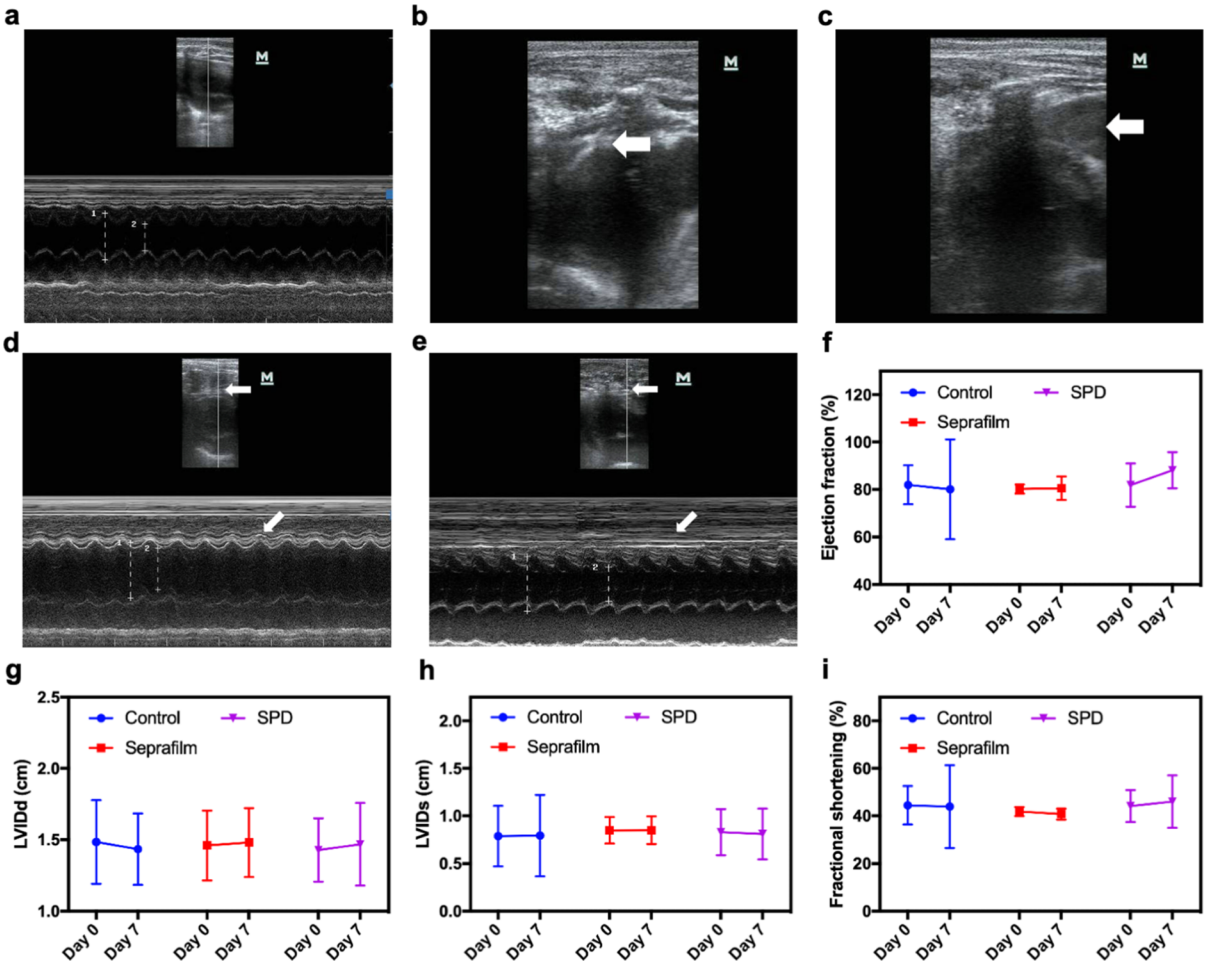

Figure 8. Echocardiographic assessment of cardiac function. (a) Representative image of a normal echocardiogram before surgery (day 0); pericardial and epicardial layers without any hypoechoic structures located in the intrapericardial region can be observed. (b) Representative image of an intrapericardial adhesion detected by echocardiography as an echolucent structure (white arrow) during the seventh postoperative day of the control group. (c) Pericardial effusion was detected in a non-treated animal (control group) after 7 days, as indicated by a white arrow that points to an echo-free signal region located in the intrapericardial space. (d) The presence of SPD was confirmed by a hypoechoic liquid located in the intrapericardial space after the first postoperative hour and (e) 7 days posterior to the surgical intervention (white arrows pointing the M mode and 2D mode). Cardiac systolic and diastolic function was measured and analyzed before surgery and 7 days after surgery in all animal groups. The application of SPD into the intrapericardial space did not show a significant impact on (f) LVEF, (g) LVIDd, (h) LVIDs, and (i) fractional shortening when compared to the other groups. Data are expressed as mean ± SD, $n = 5$ for (f–i). *P*-values were determined by Student's *t*-test and two-way ANOVA (ns: $P > 0.05$).

(Laponite XLG, BYK, Wesel, Germany), poly(ethylene oxide) (PEO) (average Mn 20,000) (Sigma-Aldrich, St. Louis, MO), and DEX (Sigma-Aldrich, St. Louis, MO) at different percentages. DEX was loaded into SNDs with a weight ratio of 1:10 by stirring (400 rpm) both components on a water solution at room temperature for 12 h. After a transparent solution was obtained, PEO was added to the solution and stirred (400 rpm) for 30 min. Several hydrogel formulations were fabricated for this study: S (11 wt % SNDs), SP (11 wt % SNDs and 5 wt % PEO), and SPD (11 wt % SNDs, 5 wt % PEO, and 0.05 wt % DEX).

Cell Culture Supplies. For the purpose of this study, NIH 3T3 fibroblasts and bEnd.3 mouse brain endothelial cells (ATCC, Manassas, VA) were used and cultured in DMEM (Thermo Fisher Scientific, Waltham, MA) containing 10% fetal bovine serum (FBS) (Thermo Fisher Scientific, Waltham, MA) under 5% CO_2 at 37 °C, and mIMCD-3 epithelial cells (ATCC, Manassas, VA) were used and cultured in DMEM nutrient mixture F-12 (Thermo Fisher Scientific, Waltham, MA) containing 10% fetal bovine serum under 5% CO_2 at 37 °C. TNF-α (R&D Systems, Minneapolis, MN) (10 ng/mL) was used to stimulate a cellular inflammatory state.

Rheological Analysis of Hydrogel Compositions. To perform the rheological analysis of hydrogel compositions, an AR-G2 rheometer (TA instruments, New Castile, DE) was used. All tests were performed on a 40 mm diameter conical plate (1° inclination and 50 μm of gap height), and to prevent water evaporation, mineral oil was placed around it. An equilibration time of 10 min followed by the application of shear at 10 s^{-1} for 2 min was used. Frequency sweeps (0.01–100 Hz at 1% strain), shear rate sweeps (0.1–1000^{-1} with 10 points/decade), stress sweep (0.1–1000 Pa), and strain sweeps (0.0001–1000% at 1 Hz) were performed at a temperature of 37 °C. Recovery analysis was done by applying several cycles of strain that were located inside (1%) and outside (100%) the value of the linear viscoelastic range. Creep was measured by applying different stress (σ) ranges (10, 20, and 30 Pa) to the hydrogel composition for 30 min, followed by a 30 min relaxation period and posterior analysis of the resulting strain (ε).

Environmental SEM Imaging. An FEI/Philips XL30 FEG ESEM (FEI/Phillips, Hillsboro, OR) was used to image hydrogels and determine their morphological features on a hydrated state. Hydrogel samples were longitudinally and transversely sectioned before the

https://doi.org/10.1021/acsami.0c20084
ACS Appl. Mater. Interfaces XXXX, XXX, XXX–XXX

analysis and mounted on a holder containing carbon tape for posterior imaging.

Injection Force Characterization. To analyze the required injection force to extrude the hydrogel formulations from a syringe, a mechanical tester (Zwick/Roell Z010) (ZwickRoell, Kennesaw, GA) was used. Hydrogel formulations were loaded and injected through 3 mL syringes (BD Biosciences, San Jose, CA) incorporated with three needle sizes [intraluminal diameters of 0.838 mm (18G), 0.337 mm (23G), and 0.260 mm (26G)] (BD Biosciences, San Jose, CA). The lower housing of the syringe was fixed on the tensile grip of the instrument to prevent any movement and the plunger was pressed by the upper compression platen at a rate of 2 mL/min. To determine the extrusion force, a 100-N load cell was used. All experiments were performed in triplicate and analyzed using testXpert software (ZwickRoell, Kennesaw, GA).

Spread Area and Stiffness Analysis. The spread area and stiffness of hydrogel formulations were evaluated 48 h after their fabrication. All hydrogel formulations were incubated for 1 h at 37 °C, and after incubation, the studies were quickly performed at room temperature. Hydrogel formulations were placed between two horizontal transparent glass plates (Bio-Rad, Hercules, CA), and a pre-determined mass (125, 250, 375, 500, 625, 750, 875, and 1000 g) was placed on the upper plate. After 5 minutes, the weight was removed, and the spreading diameter was measured. The spreadability was quantified as the total area covered by the hydrogel within the plates, and its fluidity and stiffness classified according to a previous published work.[32,33]

Hydrogel Swelling and Degradation Test. To analyze the swelling behavior of hydrogels, 1 mL of each hydrogel formulation was incubated on 5 mL of PBS (Thermo Fisher Scientific, Waltham, MA) and 5 mL of DMEM (Thermo Fisher Scientific, Waltham, MA) at 37 °C on separate 35 mm Petri dishes (Thermo Fisher Scientific, Waltham, MA). For a period of 14 days, hydrogels were weighed at predetermined timepoints. Swelling rate was calculated by using the following equation: $(W_t - W_0)/W_0 \times 100\%$, where W_0 represents the initial weight and W_t represents the weight measured during each timepoint. Degradation of mass percentage was calculated by using the following equation: $W_t/W_0 \times 100\%$.

^{1}H Nuclear Magnetic Resonance Analysis. For the ^{1}H NMR analysis, individual components as well as the finalized hydrogel system were dissolved in deuterated methanol (CD_3OD) (Sigma-Aldrich, St. Louis, MO) and deuterium oxide (D_2O) (Sigma-Aldrich, St. Louis, MO) at a concentration of 30 mg/mL. The analysis of the samples was performed at 25 °C on a Bruker AVANCE (400 MHz) spectrometer (Bruker, Harvard, MA). The chemical shifts were reported in ppm, and the solvent resonance resulting from incomplete deuterium incorporation was employed as the internal standard (CD_3OD: δ = 3.31 ppm or D_2O: δ = 4.79 ppm). The data were processed using TopSpin 3.6.1 software (Bruker, Harvard, MA) by comparing the hydrogel composition with the respective starting materials, chemical shifts, and multiplicity (s = singlet, d = doublet, q = quartet, br = broad, and m = multiplet).

DEX Release Kinetics. To determine the release kinetics of DEX, 3 mL of the drug-loaded hydrogel composition was placed inside a Spectra/Por Dialysis Tube (Repligen Corporation, Waltham, MA) and incubated on a PBS solution at 37 °C under rotatory shaking (70 rpm). At predetermined timepoints (1, 3, 6, 12, 24, 72, and 120 h), the PBS solution outside of the dialysis membrane was analyzed via UV−vis spectroscopy to determine the concentration of the released drug.

Cellular Morphological Analysis. A morphological analysis (aspect ratio and area) of cells seeded in different surfaces was performed to determine their adhesion to different substrates. Briefly, NIH 3T3 fibroblasts (10×10^4) were seeded on the surface of S, SP, and SPD hydrogels and compared to cells seeded in a standard polystyrene surface for cell growth (Corning Inc., Corning, NY). After a period of 24 h, cells were fixed and Phalloidin (green) (Thermo Fisher Scientific, Waltham, MA) staining was performed. Micrographs were captured using a confocal microscope (Carl Zeiss LSM700, Zaventem, Belgium) and analyzed via ImageJ (National Institutes of Health, Bethesda, MD). The maximum orthogonal length, width, and area of 60 individual cells were analyzed, and the aspect ratio was calculated using these parameters as previously described.[55]

Cellular Viability Test. The cytotoxicity of hydrogel compositions was evaluated by seeding NIH 3T3 fibroblasts (10×10^3) and mIMCD-3 epithelial cells (10×10^3) in 96-well culture plates (Corning Inc., Corning, NY) and incubating them with several concentration ranges (0.001−1000 μg/mL) of S, SP, and SPD hydrogels for 48 h. The PrestoBlue Cell Viability Assay (Thermo Fisher Scientific, Waltham, MA) was used, and cytotoxicity was measured via a microplate reader (Infinite M200 Tecan, Männedorf, Switzerland) and analyzed through the i-Control software (Tecan, Männedorf, Switzerland).

***In Vitro* Anti-inflammatory Assessment.** To simulate the protective anti-inflammatory response of DEX, mouse brain endothelial cells (bEnd.3) were seeded into an eight-well chamber slide (Thermo Scientific, Waltham, MA) at a density of 2×10^3 per well. Three hours before performing TNF-α (10 ng/mL) stimulation, free DEX (50 mM), SP, and the DEX-loaded (50 mM) hydrogel (SPD) were added as pretreatments to the media of different groups. After 8 h, cells were fixed, and immunohistochemistry was performed to determine the upregulation of cellular inflammatory markers (ICAM-1 and VCAM-1). Anti-ICAM-1 antibody (Abcam, Cambridge, MA) and anti-VCAM-1 antibody (Abcam, Cambridge, MA) were used to visualize cellular expression of these inflammatory markers. Images were captured via confocal microscopy (Carl Zeiss LSM700, Zaventem, Belgium) and analyzed via ZEN software (Carl Zeiss, Zaventem, Belgium).

Intrapericardial Adhesion Animal Model. An intrapericardial adhesion animal model was used to test the efficacy of the hydrogel formulations. Four month old male Japanese white rabbits (body weight 2−2.2 kg) were purchased from Huazhong Agricultural University Laboratory Animal Center and divided into four groups with five animals per group under controlled environmental conditions (22−24 °C, 50−60% humidity) with standard diet. The animal research protocol was approved by the Institutional Animal Care and Use Research Committee of Tongji Medical College prior to initiation of the study, and all animal experiments were conducted according to the NIH Guidelines for the Care and Use of Laboratory Animals. Rabbits were first anesthetized with 3% pentobarbital sodium (1 mL/kg), and a costal sternotomy in the left side was performed through a 4 cm incision at the level of the fourth intercostal space. A sternal retractor was placed, and the anterior pericardium was exposed and opened approximately 2 cm in length to reveal the anterior surface of the heart. After opening the intrapericardial space, superficial needle (23G) punctures in four different areas of the left ventricular epicardium were performed without perforating the muscular wall, as previously described in a similar animal model.[50] Before the surgical incision was closed, different groups received a specific type of treatment administered in the intrapericardial space, the control group received 0.1 mL of saline solution, a positive control group received Seprafilm, and the last group was administered with the DEX-loaded hydrogel (SPD). Finally, the sternotomy was repaired by suturing the different pericardial, muscular, and skin layers separately. Animals were kept alive for 7 days before adhesion formation was assessed after euthanasia.

Evaluation of Intrapericardial Adhesions. Intrapericardial adhesions were assessed by a modified version of the PAI applied to the pericardium to grade the severity of adhesions based on morphological features such as vascularization, thickness, and strength.[52] The scoring system classifies adhesion grades as follows: 0—no adhesion, 1—filmy adhesion that needs blunt dissection, 2—strong adhesion that needs sharp dissection, and 3—very strong vascularized adhesion that needs sharp dissection with damage hardly preventable. The four injury sites in the epicardial region were individually graded, and the total score was calculated. The percentage of adhesion formation and adhesion area was also calculated based on the number of adhesions formed; each of the four injury sites were

https://doi.org/10.1021/acsami.0c20084
ACS Appl. Mater. Interfaces XXXX, XXX, XXX−XXX

considered as 25% of the total surface area present in the injured epicardium.

Histopathological Examination of Postoperative Adhesions. After tissue extraction, H&E (Sigma-Aldrich, St. Louis, MO), and Masson's trichrome (Sigma-Aldrich, St. Louis, MO) staining were performed in paraffin sections to evaluate tissue morphology and fibrotic remodeling. Microscopic images were captured via a Pannoramic SCAN II (3DHistech, Budapest, Hungary) imaging system.

Immunohistological Analysis. Immunohistological staining was performed by using CD3 (Abcam, ab135372, diluted 1:100), CD68 (Abcam 222914, diluted 1:100), and NF-KB (Bioss, Bs-0465R, diluted 1:100) primary antibodies and 488-labeled anti-mouse (Aspen, AS-1110, diluted 1:50) and CY3-labeled anti-rabbit (Aspen, AS-1110, diluted 1:50) secondary antibodies. Nuclei were stained using DAPI (Life Technologies, diluted 1:1000). Tissue sections were imaged using a confocal microscopy system (Carl Zeiss LSM700, Zaventem, Belgium), and ZEN software (Carl Zeiss, Zaventem, Belgium) was used for image analysis.

Evaluation of Systemic Inflammation. Two milliliters of blood were obtained from the auricular vein of the animals in two timepoints, before performing the surgical procedure and after 7 postoperative days. ESR was measured by a specialized blood sedimentation kit (Xin Kang Medical, Taizhou, China) according to the Westergren method. The concentration of CRP was determined by a sandwich ELISA kit (SEA821Rb 96T, Cloud-Cone Corp., Katy, TX) according to manufacturer instructions.

Echocardiographic Evaluation. Echocardiographic studies were performed to analyze the presence of postoperative adhesions as well as the systolic and diastolic function of the heart before the surgical procedure and 1 h and 7 days after performing the surgical intervention. Anesthesia was administered via intraperitoneal injection (3% pentobarbital, 1 mL/kg), and a transthoracic 2D guided M-mode echocardiography system (DP-50Vet, Mindray, Shenzhen, China) was used to analyze the cardiac cycle. The cardiac long axis (at the papillary level) was used to measure mean LVEF, LVIDd, LVIDs, and FS during five cardiac cycles.

Statistical Analysis. Statistical significance was determined by using unpaired Student's *t*-test and one-way ANOVA in all samples and groups. All the results in this study are expressed as mean ± SD. $^{*}P < 0.05$ and $^{**}P < 0.01$ are considered statistically significant.

■ ASSOCIATED CONTENT

Supporting Information

The Supporting Information is available free of charge at https://pubs.acs.org/doi/10.1021/acsami.0c20084.

Structural characterization of SND; rheological assessment of DLSH formulations; mechanical tester instrument used to determine hydrogel extrusion force; representative photographs of SPD formulation after compression; hydrogel swelling test in DMEM and degradation kinetics in PBS; representative photographs of drug-loaded SPD formulation; schematic representation of the set up used to determine DEX release kinetics; representative images of the gross appearance of the cardiac samples; CRP and ESR tests; representative image of an echocardiogram of animal model; needle characteristics and extrusion speed; categorization of hydrogel stiffness; chemical shift peak of each proton corresponding to components in SPD hydrogel; and modified PAI adapted for intrapericardial adhesion grading (PDF)

Presence of fibrotic adhesions (MP4)

Thickening of the pericardium (MP4)

■ AUTHOR INFORMATION

Corresponding Authors

Guillermo U. Ruiz-Esparza − *Division of Engineering in Medicine, Department of Medicine, Brigham and Women's Hospital and Renal Division, Department of Medicine, Brigham and Women's Hospital, Harvard Medical School, Boston, Massachusetts 02115, United States; Division of Health Sciences and Technology, Harvard University - Massachusetts Institute of Technology, Cambridge, Massachusetts 02139, United States;* orcid.org/0000-0002-1064-6214; Email: gruizeh@bwh.harvard.edu, gruizeh@mit.edu

Nianguo Dong − *Department of Cardiovascular Surgery, Union Hospital, Tongji Medical College, Huazhong University of Science and Technology, Wuhan 430022, China*; Email: 1986xh0694@hust.edu.cn

Joseph V. Bonventre − *Division of Engineering in Medicine, Department of Medicine, Brigham and Women's Hospital and Renal Division, Department of Medicine, Brigham and Women's Hospital, Harvard Medical School, Boston, Massachusetts 02115, United States; Division of Health Sciences and Technology, Harvard University - Massachusetts Institute of Technology, Cambridge, Massachusetts 02139, United States*; Email: joseph_bonventre@hms.harvard.edu

Authors

Xichi Wang − *Division of Engineering in Medicine, Department of Medicine, Brigham and Women's Hospital and Renal Division, Department of Medicine, Brigham and Women's Hospital, Harvard Medical School, Boston, Massachusetts 02115, United States; Division of Health Sciences and Technology, Harvard University - Massachusetts Institute of Technology, Cambridge, Massachusetts 02139, United States; Department of Cardiovascular Surgery, Union Hospital, Tongji Medical College, Huazhong University of Science and Technology, Wuhan 430022, China*

Zongtao Liu − *Department of Cardiovascular Surgery, Union Hospital, Tongji Medical College, Huazhong University of Science and Technology, Wuhan 430022, China*

Diego A. Sandoval-Salaiza − *Division of Engineering in Medicine, Department of Medicine, Brigham and Women's Hospital and Renal Division, Department of Medicine, Brigham and Women's Hospital, Harvard Medical School, Boston, Massachusetts 02115, United States; Division of Health Sciences and Technology, Harvard University - Massachusetts Institute of Technology, Cambridge, Massachusetts 02139, United States; School of Engineering and Science, Tecnologico de Monterrey, Monterrey, Nuevo Leon 64849, Mexico*

Samson Afewerki − *Division of Engineering in Medicine, Department of Medicine, Brigham and Women's Hospital, Harvard Medical School, Boston, Massachusetts 02115, United States; Division of Health Sciences and Technology, Harvard University - Massachusetts Institute of Technology, Cambridge, Massachusetts 02139, United States; Department of Chemical Engineering and Koch Institute for Integrative Cancer Research, Massachusetts Institute of Technology, Cambridge, Massachusetts 02139, United States*

Mildred G. Jimenez-Rodriguez − *Division of Engineering in Medicine, Department of Medicine, Brigham and Women's Hospital and Renal Division, Department of Medicine, Brigham and Women's Hospital, Harvard Medical School, Boston, Massachusetts 02115, United States; Division of*

https://doi.org/10.1021/acsami.0c20084
ACS Appl. Mater. Interfaces XXXX, XXX, XXX−XXX

Health Sciences and Technology, Harvard University - Massachusetts Institute of Technology, Cambridge, Massachusetts 02139, United States; School of Engineering and Science, Tecnologico de Monterrey, Monterrey, Nuevo Leon 64849, Mexico

Lorena Sanchez-Melgar − *Division of Engineering in Medicine, Department of Medicine, Brigham and Women's Hospital and Renal Division, Department of Medicine, Brigham and Women's Hospital, Harvard Medical School, Boston, Massachusetts 02115, United States; Division of Health Sciences and Technology, Harvard University - Massachusetts Institute of Technology, Cambridge, Massachusetts 02139, United States; School of Engineering and Science, Tecnologico de Monterrey, Monterrey, Nuevo Leon 64849, Mexico*

Gabriela Güemes-Aguilar − *Division of Engineering in Medicine, Department of Medicine, Brigham and Women's Hospital and Renal Division, Department of Medicine, Brigham and Women's Hospital, Harvard Medical School, Boston, Massachusetts 02115, United States; Division of Health Sciences and Technology, Harvard University - Massachusetts Institute of Technology, Cambridge, Massachusetts 02139, United States; School of Medicine and Health Science, Tecnologico de Monterrey, Monterrey, Nuevo Leon 64849, Mexico*

David G. Gonzalez-Sanchez − *Division of Engineering in Medicine, Department of Medicine, Brigham and Women's Hospital and Renal Division, Department of Medicine, Brigham and Women's Hospital, Harvard Medical School, Boston, Massachusetts 02115, United States; Division of Health Sciences and Technology, Harvard University - Massachusetts Institute of Technology, Cambridge, Massachusetts 02139, United States; School of Medicine and Health Science, Tecnologico de Monterrey, Monterrey, Nuevo Leon 64849, Mexico*

Oscar Noble − *Division of Engineering in Medicine, Department of Medicine, Brigham and Women's Hospital and Renal Division, Department of Medicine, Brigham and Women's Hospital, Harvard Medical School, Boston, Massachusetts 02115, United States; Division of Health Sciences and Technology, Harvard University - Massachusetts Institute of Technology, Cambridge, Massachusetts 02139, United States; School of Medicine and Health Science, Tecnologico de Monterrey, Monterrey, Nuevo Leon 64849, Mexico*

Cecilia Lerma − *Division of Engineering in Medicine, Department of Medicine, Brigham and Women's Hospital and Renal Division, Department of Medicine, Brigham and Women's Hospital, Harvard Medical School, Boston, Massachusetts 02115, United States; Division of Health Sciences and Technology, Harvard University - Massachusetts Institute of Technology, Cambridge, Massachusetts 02139, United States; School of Engineering and Science, Tecnologico de Monterrey, Monterrey, Nuevo Leon 64849, Mexico*

Roberto Parra-Saldivar − *Division of Engineering in Medicine, Department of Medicine, Brigham and Women's Hospital, Harvard Medical School, Boston, Massachusetts 02115, United States; Division of Health Sciences and Technology, Harvard University - Massachusetts Institute of Technology, Cambridge, Massachusetts 02139, United States; School of Engineering and Science, Tecnologico de Monterrey, Monterrey, Nuevo Leon 64849, Mexico*

Dario R. Lemos − *Division of Engineering in Medicine, Department of Medicine, Brigham and Women's Hospital and Renal Division, Department of Medicine, Brigham and Women's Hospital, Harvard Medical School, Boston, Massachusetts 02115, United States*

Guillermo A. Llamas-Esperon − *Department of Interventional Cardiology, Hospital Cardiológica, Aguascalientes 20230, Mexico*

Jiawei Shi − *Department of Cardiovascular Surgery, Union Hospital, Tongji Medical College, Huazhong University of Science and Technology, Wuhan 430022, China*

Li Li − *Renal Division, Department of Medicine, Brigham and Women's Hospital, Harvard Medical School, Boston, Massachusetts 02115, United States*

Anderson O. Lobo − *LIMAV—Interdisciplinary Laboratory for Advanced Materials, BioMatLab group, Material Science and Engineering Graduate Program, UFPI- Federal University of Piauí, Teresina, Piauí 64049−550, Brazil;* orcid.org/0000-0002-2544-0438

Andres A. Fuentes-Baldemar − *Division of Engineering in Medicine, Department of Medicine, Brigham and Women's Hospital and Renal Division, Department of Medicine, Brigham and Women's Hospital, Harvard Medical School, Boston, Massachusetts 02115, United States; Division of Health Sciences and Technology, Harvard University - Massachusetts Institute of Technology, Cambridge, Massachusetts 02139, United States*

Complete contact information is available at: https://pubs.acs.org/10.1021/acsami.0c20084

Author Contributions

X.W. and Z.L. authors contributed equally to this work. X.W. and G.U.R-E. conceived the project. X.W., Z.L., J.V.B, N.D., and G.U.R-E performed the experimental design. X.W., Z.L., D.A.S.-S., S.A., M.G.J-R., L.S-M., G.G-A., D.G.G-S., O.N., C.L., R.P-S., D.R.L., G.A.L-E., J.S., M.F., L.L., and A.A.F-B. performed the experiments. X.W., Z.L., D.A.S-A., S.A., M.G.J-R., L.S-M., G.G-A., D.G.G-S., O.N., C.L., R.P-S., D.R.L., G.A.L-E., J.S., M.F., L.L., A.A.F-B., Z.L., J.V.B, N.D., and G.U.R-E analyzed the data.

Notes

The authors declare no competing financial interest.

■ ACKNOWLEDGMENTS

X.W. acknowledges the support from the Department of Cardiovascular Surgery, Union Hospital, Tongji Medical College, Huazhong University of Science and Technology, and the National Key Research and Development Program of China (2016YFA0101100). The authors acknowledge the financial and scientific support of Brigham and Women's Hospital, Harvard Medical School, Massachusetts Institute of Technology, Huazhong University of Science and Technology, and the Tecnologico de Monterrey—MIT Nanotechnology Program.

■ REFERENCES

(1) Capella-Monsonís, H.; Kearns, S.; Kelly, J.; Zeugolis, D. I. Battling Adhesions: From Understanding to Prevention. *BMC Biom. Eng.* **2019**, *1*, 5.

(2) Park, C. B.; Suri, R. M.; Burkhart, H. M.; Greason, K. L.; Dearani, J. A.; Schaff, H. V.; Sundt, T. M., III Identifying Patients at Particular Risk of Injury During Repeat Sternotomy: Analysis of 2555

Cardiac Reoperations. *J. Thorac. Cardiovasc. Surg.* **2010**, *140*, 1028−1035.
(3) Sikirica, V.; Bapat, B.; Candrilli, S. D.; Davis, K. L.; Wilson, M.; Johns, A. The Inpatient Burden of Abdominal and Gynecological Adhesiolysis in the US. *BMC Surg.* **2011**, *11*, 13.
(4) Anyanwu, A. C. Technique for less invasive implantation of Heartmate II left ventricular assist device without median sternotomy. *Seminars in Thoracic and Cardiovascular Surgery*; Elsevier, 2011; pp 241−244.
(5) Roselli, E. E.; Pettersson, G. B.; Blackstone, E. H.; Brizzio, M. E.; Houghtaling, P. L.; Hauck, R.; Burke, J. M.; Lytle, B. W. Adverse Events During Reoperative Cardiac Surgery: Frequency, Characterization, and Rescue. *J. Thorac. Cardiovasc. Surg.* **2008**, *135*, 316−323.
(6) Hoit, B. D. Pathophysiology of the Pericardium. *Prog. Cardiovasc. Dis.* **2017**, *59*, 341−348.
(7) Cannata, A.; Petrella, D.; Russo, C. F.; Bruschi, G.; Fratto, P.; Gambacorta, M.; Martinelli, L. Postsurgical Intrapericardial Adhesions: Mechanisms of Formation and Prevention. *Ann. Thorac. Surg.* **2013**, *95*, 1818−1826.
(8) Van Baal, J. O. A. M.; Van de Vijver, K. K.; Nieuwland, R.; Van Noorden, C. J. F.; Van Driel, W. J.; Sturk, A.; Kenter, G. G.; Rikkert, L. G.; Lok, C. A. R. The Histophysiology and Pathophysiology of the Peritoneum. *Tissue Cell* **2017**, *49*, 95−105.
(9) Rout, U. K.; Diamond, M. P. Role of Plasminogen Activators during Healing after Uterine Serosal Lesioning in the Rat. *Fertil. Steril.* **2003**, *79*, 138−145.
(10) Lorini, F. L.; Cerutti, S.; Di Dedda, G. Pericardium and Pericardial Disease. *Textbook of Echocardiography for Intensivists and Emergency Physicians*; Springer, 2019; pp 117−123.
(11) Tissot, C.; Phelps, C. M.; da Cruz, E. M.; Miyamoto, S. D. Pericardial Diseases. In *Critical Care of Children with Heart Disease*; Springer, 2020; pp 503−522.
(12) Van Der Krabben, A. A.; Dijkstra, F. R.; Nieuwenhuijzen, M.; Reijnen, M. M. P. J.; Schaapveld, M.; Van Goor, H. Morbidity and Mortality of Inadvertent Enterotomy during Adhesiotomy. *Br. J. Surg.* **2000**, *87*, 467−471.
(13) van der Linden, J.; Duvernoy, O.; Hadjinikolaou, L.; Bengtsson, L. Does hyaluronate prevent postoperative retro-sternal adhesions in coronary surgery? - Preliminary results. *Eur. J. Cardio. Thorac. Surg.* **2001**, *19*, 949−950.
(14) Lih, E.; Oh, S. H.; Joung, Y. K.; Lee, J. H.; Han, D. K. Polymers for Cell/tissue Anti-adhesion. *Prog. Polym. Sci.* **2015**, *44*, 28−61.
(15) Stapleton, L. M.; Steele, A. N.; Wang, H.; Lopez Hernandez, H.; Yu, A. C.; Paulsen, M. J.; Smith, A. A. A.; Roth, G. A.; Thakore, A. D.; Lucian, H. J.; Totherow, K. P.; Baker, S. W.; Tada, Y.; Farry, J. M.; Eskandari, A.; Hironaka, C. E.; Jaatinen, K. J.; Williams, K. M.; Bergamasco, H.; Marschel, C.; Chadwick, B.; Grady, F.; Ma, M.; Appel, E. A.; Woo, Y. J. Use of a Supramolecular Polymeric Hydrogel As an Effective Post-operative Pericardial Adhesion Barrier. *Nat. Biomed. Eng.* **2019**, *3*, 611−620.
(16) Zeng, Q.; Yu, Z.; You, J.; Zhang, Q. Efficacy and Safety of Seprafilm for Preventing Postoperative Abdominal Adhesion: Systematic Review and Meta-analysis. *World J. Surg.* **2007**, *31*, 2125−2131.
(17) Trew, G.; Pistofidis, G.; Pados, G.; Lower, A.; Mettler, L.; Wallwiener, D.; Korell, M.; Pouly, J. L.; Coccia, M. E.; Audebert, A.; Nappi, C.; Schmidt, E.; McVeigh, E.; Landi, S.; Degueldre, M.; Koninckx, P.; Rimbach, S.; Chapron, C.; Dallay, D.; Röemer, T.; McConnachie, A.; Ford, I.; Crowe, A.; Knight, A.; Dizerega, G.; Dewilde, R. Gynaecological Endoscopic Evaluation of 4% Icodextrin Solution: A European, Multicentre, Double-blind, Randomized Study of the Efficacy and Safety in the Reduction of de novo Adhesions after Laparoscopic Gynaecological Surgery. *Hum. Reprod.* **2011**, *26*, 2015−2027.
(18) Becher, T. B.; Braga, C. B.; Bertuzzi, D. L.; Ramos, M. D.; Hassan, A.; Crespilho, F. N.; Ornelas, C. The structure-property relationship in LAPONITE materials: from Wigner glasses to strong self-healing hydrogels formed by non-covalent interactions. *Soft Matter* **2019**, *15*, 1278−1289.
(19) Murphy, G. S.; Sherwani, S. S.; Szokol, J. W.; Avram, M. J.; Greenberg, S. B.; Patel, K. M.; Wade, L. D.; Vaughn, J.; Gray, J. Small-dose Dexamethasone Improves Quality of Recovery Scores after Elective Cardiac Surgery: a Randomized, Double-blind, Placebo-controlled Study. *J. Cardiothorac. Vasc. Anesth.* **2011**, *25*, 950−960.
(20) Sheikhi, A.; Afewerki, S.; Oklu, R.; Gaharwar, A. K.; Khademhosseini, A. Effect of ionic strength on shear-thinning nanoclay-polymer composite hydrogels. *Biomater. Sci.* **2018**, *6*, 2073−2083.
(21) Yan, C.; Pochan, D. J. Rheological Properties of Peptide-based Hydrogels for Biomedical and Other Applications. *Chem. Soc. Rev.* **2010**, *39*, 3528−3540.
(22) Liu, X.; Bhatia, S. R. Laponite and Laponite-PEO hydrogels with enhanced elasticity in phosphate-buffered saline. *Polym. Adv. Technol.* **2015**, *26*, 874−879.
(23) Roozbahani, M.; Kharaziha, M.; Emadi, R. pH Sensitive Dexamethasone Encapsulated Laponite Nanoplatelets: Release Mechanism and Cytotoxicity. *Int. J. Pharm.* **2017**, *518*, 312−319.
(24) Gaharwar, A. K.; Schexnailder, P. J.; Kline, B. P.; Schmidt, G. Assessment of using Laponite cross-linked poly(ethylene oxide) for controlled cell adhesion and mineralization. *Acta Biomater.* **2011**, *7*, 568−577.
(25) Papanicolaou, G. C.; Zaoutsos, S. P. 1—Viscoelastic Constitutive Modeling of Creep and Stress Relaxation in Polymers and Polymer Matrix Composites. In *Creep and Fatigue in Polymer Matrix Composites*; Guedes, R. M., Ed.; Woodhead Publishing, 2011; pp 3−47.
(26) Ahearne, M.; Yang, Y.; El Haj, A. J.; Then, K. Y.; Liu, K.-K. Characterizing the Viscoelastic Properties of Thin Hydrogel-based Constructs for Tissue Engineering Applications. *J. R. Soc. Interface* **2005**, *2*, 455−463.
(27) Dammers, R.; Stifft, F.; Tordoir, J. H. M.; Hameleers, J. M. M.; Hoeks, A. P. G.; Kitslaar, P. J. E. H. M. Shear Stress Depends on Vascular Territory: Comparison between Common Carotid and Brachial Artery. *J. Appl. Physiol.* **2003**, *94*, 485−489.
(28) Pinto, J. G.; Patitucci, P. J. Creep in Cardiac Muscle. *Am. J. Physiol. Heart Circ. Physiol.* **1977**, *232*, H553−H563.
(29) Kwak, B. R.; Bäck, M.; Bochaton-Piallat, M.-L.; Caligiuri, G.; Daemen, M. J. A. P.; Davies, P. F.; Hoefer, I. E.; Holvoet, P.; Jo, H.; Krams, R.; Lehoux, S.; Monaco, C.; Steffens, S.; Virmani, R.; Weber, C.; Wentzel, J. J.; Evans, P. C. Biomechanical factors in atherosclerosis: mechanisms and clinical implications. *Eur. Heart J.* **2014**, *35*, 3013−3020.
(30) Dhawan, S. S.; Avati Nanjundappa, R. P.; Branch, J. R.; Taylor, W. R.; Quyyumi, A. A.; Jo, H.; McDaniel, M. C.; Suo, J.; Giddens, D.; Samady, H. Shear Stress and Plaque Development. *Expet Rev. Cardiovasc. Ther.* **2010**, *8*, 545−556.
(31) Tomás, H.; Alves, C. S.; Rodrigues, J. Laponite: A key nanoplatform for biomedical applications? *Nanomed. Nanotechnol. Biol. Med.* **2018**, *14*, 2407−2420.
(32) El-Kased, R. F.; Amer, R. I.; Attia, D.; Elmazar, M. Honey-based Hydrogel: In vitro and Comparative In vivo Evaluation for Burn Wound Healing. *Sci. Rep.* **2017**, *7*, 9692.
(33) Garg, A.; Aggarwal, D.; Garg, S.; Singla, A. K. Spreading of Semisolid Formulations: An Update. *Pharmaceut. Technol. N. Am.* **2002**, *26*, 84.
(34) Lee, S. H.; Lee, W. J.; Kim, T. K.; Bayazit, M. K.; Kim, S. O.; Choi, Y. S. UV-crosslinked poly(arylene ether sulfone) - LAPONITE nanocomposites for proton exchange membranes. *RSC Adv.* **2017**, *7*, 28358−28365.
(35) López-Angulo, D.; Bittante, A. M. Q. B.; Luciano, C. G.; Ayala-Valencia, G.; Flaker, C. H. C.; Djabourov, M.; José do Amaral Sobral, P. Effect of Laponite on the structure, thermal stability and barrier properties of nanocomposite gelatin films. *Food Biosci.* **2020**, *35*, 100596.
(36) Wang, S.; Zheng, F.; Huang, Y.; Fang, Y.; Shen, M.; Zhu, M.; Shi, X. Encapsulation of Amoxicillin within Laponite-Doped Poly(lactic-co-glycolic acid) Nanofibers: Preparation, Characterization,

https://doi.org/10.1021/acsami.0c20084
ACS Appl. Mater. Interfaces XXXX, XXX, XXX−XXX

and Antibacterial Activity. *ACS Appl. Mater. Interfaces* **2012**, *4*, 6393−6401.
(37) Ghadiri, M.; Hau, H.; Chrzanowski, W.; Agus, H.; Rohanizadeh, R. Laponite Clay As a Carrier for in situ Delivery of Tetracycline. *RSC Adv.* **2013**, *3*, 20193−20201.
(38) Fraile, J. M.; Garcia-Martin, E.; Gil, C.; Mayoral, J. A.; Pablo, L. E.; Polo, V.; Prieto, E.; Vispe, E. Laponite as Carrier for Controlled in vitro Delivery of Dexamethasone in Vitreous Humor Models. *Eur. J. Pharm. Biopharm.* **2016**, *108*, 83−90.
(39) Jung, H.; Kim, H.-M.; Choy, Y. B.; Hwang, S.-J.; Choy, J.-H. Itraconazole-Laponite: Kinetics and mechanism of drug release. *Appl. Clay Sci.* **2008**, *40*, 99−107.
(40) Midelfart, A.; Dybdahl, A.; Müller, N.; Sitter, B.; Gribbestad, I. S.; Krane, J. Dexamethasone and Dexamethasone Phosphate Detected by1H and19F NMR Spectroscopy in the Aqueous Humour. *Exp. Eye Res.* **1998**, *66*, 327−337.
(41) Roozbahani, M.; Kharaziha, M.; Emadi, R. pH Sensitive Dexamethasone Encapsulated Laponite Nanoplatelets: Release Mechanism and Cytotoxicity. *Int. J. Pharm.* **2017**, *518*, 312−319.
(42) Dawson, J. I.; Oreffo, R. O. C. Clay: New Opportunities for Tissue Regeneration and Biomaterial Design. *Adv. Mater.* **2013**, *25*, 4069−4086.
(43) Polderman, J. A. W.; Farhang-Razi, V.; Dieren, S.; Kranke, P.; DeVries, J. H.; Hollmann, M. W.; Preckel, B.; Hermanides, J. Adverse side-effects of dexamethasone in surgical patients - an abridged Cochrane systematic review. *Anaesthesia* **2019**, *74*, 929−939.
(44) Cannata, A.; Petrella, D.; Russo, C. F.; Bruschi, G.; Fratto, P.; Gambacorta, M.; Martinelli, L. Postsurgical Intrapericardial Adhesions: Mechanisms of Formation and Prevention. *Ann. Thorac. Surg.* **2013**, *95*, 1818−1826.
(45) Li, J.; Feng, X.; Liu, B.; Yu, Y.; Sun, L.; Liu, T.; Wang, Y.; Ding, J.; Chen, X. Polymer Materials for Prevention of Postoperative Adhesion. *Acta Biomater.* **2017**, *61*, 21−40.
(46) Krawinkel, J.; Torres-Mapa, M.; Werelius, K.; Heisterkamp, A.; Rüttermann, S.; Romanos, G.; Gerhardt-Szép, S. Gold Nanoparticle-mediated Delivery of Molecules into Primary Human Gingival Fibroblasts Using Ns-laser Pulses: A Pilot Study. *Materials* **2016**, *9*, 397.
(47) Jacob, K. A.; Leaf, D. E.; Dieleman, J. M.; van Dijk, D.; Nierich, A. P.; Rosseel, P. M.; van der Maaten, J. M.; Hofland, J.; Diephuis, J. C.; de Lange, F.; Boer, C.; Kluin, J.; Waikar, S. S. Intraoperative High-dose Dexamethasone and Severe AKI after Cardiac Surgery. *J. Am. Soc. Nephrol.* **2015**, *26*, 2947−2951.
(48) Liu, X.; Pan, L.; Wang, X.; Gong, Q.; Zhu, Y. Z. Leonurine protects against tumor necrosis factor-α-mediated inflammation in human umbilical vein endothelial cells. *Atherosclerosis* **2012**, *222*, 34−42.
(49) Yeh, R.; Tay, Y.-K. D.; Tabacco, G.; Dercle, L.; Kuo, J. H.; Bandeira, L.; McManus, C.; Leung, D. K.; Lee, J. A.; Bilezikian, J. P. Diagnostic Performance of 4D CT and Sestamibi SPECT/CT in Localizing Parathyroid Adenomas in Primary Hyperparathyroidism. *Radiology* **2019**, *291*, 469.
(50) Feng, B.; Wang, S.; Hu, D.; Fu, W.; Wu, J.; Hong, H.; Domian, I. J.; Li, F.; Liu, J. Bioresorbable Electrospun Gelatin/polycaprolactone Nanofibrous Membrane As a Barrier to Prevent Cardiac Postoperative Adhesion. *Acta Biomater.* **2019**, *83*, 211−220.
(51) Gonzalez, A. C. d. O.; Costa, T. F.; Andrade, Z. d. A.; Medrado, A. R. A. P. Wound Healing - A Literature Review. *An. Bras. Dermatol.* **2016**, *91*, 614−620.
(52) Coccolini, F.; Ansaloni, L.; Manfredi, R.; Campanati, L.; Poiasina, E.; Bertoli, P.; Capponi, M. G.; Sartelli, M.; Saverio, S. D.; Cucchi, M.; Lazzareschi, D.; Pisano, M.; Catena, F. Peritoneal Adhesion Index (PAI): Proposal of a Score for the "Ignored Iceberg" of Medicine and Surgery. *World J. Emerg. Surg.* **2013**, *8*, 6.
(53) Al-Harbi, N. O.; Imam, F.; Al-Harbi, M. M.; Ansari, M. A.; Zoheir, K. M. A.; Korashy, H. M.; Sayed-Ahmed, M. M.; Attia, S. M.; Shabanah, O. A.; Ahmad, S. F. Dexamethasone Attenuates LPS-induced Acute Lung Injury through Inhibition of NF-κB, COX-2, and Pro-inflammatory Mediators. *Immunol. Invest.* **2016**, *45*, 349−369.
(54) Hirschelmann, A.; Tchartchian, G.; Wallwiener, M.; Hackethal, A.; De Wilde, R. L. A Review of the Problematic Adhesion Prophylaxis in Gynaecological Surgery. *Arch. Gynecol. Obstet.* **2012**, *285*, 1089−1097.
(55) Filgueira, C. S.; Igo, S. R.; Wang, D. K.; Hirsch, M.; Schulz, D. G.; Bruckner, B. A.; Grattoni, A. Technologies for Intrapericardial Delivery of Therapeutics and Cells. *Adv. Drug Delivery Rev.* **2019**, *151-152*, 222−232.

https://doi.org/10.1021/acsami.0c20084
ACS Appl. Mater. Interfaces XXXX, XXX, XXX−XXX